The Aeronautical Journal

Embedded Magnetorquer for the more Demanding Multi-Cube Small Satellites

--Manuscript Draft--

Manuscript Number:	AeroJ-2021-0163R2
Full Title:	Embedded Magnetorquer for the more Demanding Multi-Cube Small Satellites
Article Type:	Research Article
Corresponding Author:	Anwar Ali Zhejiang Sci-Tech University Hangzhou, 浙江 CHINA
Corresponding Author's Institution:	Zhejiang Sci-Tech University
Order of Authors:	Anwar Ali
	Chao Wang, BS
	Shoaib Ahmed Khan, MS
	Jijun Tong, PhD
	Leonardo Reyneri, PhD
Order of Authors Secondary Information:	
Abstract:	The recent development in the miniaturization of small satellites and their subsystems has opened a new window of research for the universities around the globe. The low-cost, lightweight, small and flexible satellites have resulted in a broad range of multi-cube format small satellites, constructed from one to many adjoined cubes, having total mass between 1 and 10 kg. The most challenging design part of the small satellites is to implant a large number of subsystems in a limited space. In order to resolve this issue, the designers are trying to shrink down the subsystem's dimensions further. In this paper, a magnetorquer coil is designed and analyzed for a 4U (4 units cube; 33×33×16.5) cm 3 and 8U (8 units cube; 33×33×33) cm 3 multi-cube small satellites respectively. The coil is embedded in the 6 internal layers of an eight-layers printed circuit board (PCB). The designed magnetorquer system is fully reconfigurable and multiple coils configurations can be achieved by attaching them in series, parallel and hybrid arrangements. Due to embedded nature, the heat generated by the coil may damage the components mounted on the PCB outer surfaces. Therefore, thermal analysis is performed to ensure that the coil generated heat will not cross the PCB components temperature safety limits. All the possible combinations of the coils are analyzed for current drawn, power consumption, heat dissipation, magnetic moment generation and resultant torque. A desired torque can be attained by using a particular coil configuration at the expense of specific amount of power consumption and PCB surface temperature rise.
Response to Reviewers:	NILL
Corresponding Author E-Mail:	safi2000pk@gmail.com
Additional Information:	
Question	**Response**
Can you confirm that you have gained all necessary copyrights and permissions to publish this manuscript legally	Yes
Has this manuscript been submitted or published in any other Journal?	No - This manuscript has not been published in another Journal
Is this manuscript the work of all the authors you have listed and have all contributing authors to this manuscript	Yes

been listed?	
Would you be interested in receiving information about subscribing to The Aeronautical Journal?	Yes
Would you be interested in receiving information about the benefits of becoming a member of The Royal Aeronautical Society?	Yes
Are you submitting any supplementary material such as additional images, extensive data sets or filmed footage, which is not essential to the main argument of your article?	No
Enter the approximate word count of the manuscript. Please note, regular papers ideally should not exceed 10,000 words while survey papers should not exceed 15,000 words. Exceeding these limits may reduce the chances of your paper being approved for publication.	4279
Are you below the age of 30 and wish to be considered for the Young Person's Written Prize Award?	No
Select the Special Issue to which you are submitting your manuscript. If you are not submitting to a Special Issue, please select "Not part of a Special Issue."	Not part of a Special Issue
Is it your intention to have your paper published under the 'Gold' option Open Access initiative, for which there is a charge?	No
Author Comments:	

Embedded Magnetorquer for the more Demanding Multi-Cube Small Satellites

Anwar Ali*, Wang Chao*, Shoaib Ahmed Khan†, Jijun Tong*, Leonardo M. Reyneri
* School of Information Science and Technology, Zhejiang Sci-Tech University, Hangzhou 310018, China
safi2000pk@gmail.com
† College of Electrical Engineering, Zhejiang University, Hangzhou, 310027, China
Department of Electronics and Telecommunications, Politecnico di Torino, Torino, Italy

***Abstract*—** The recent development in the miniaturization of small satellites and their subsystems has opened a new window of research for the universities around the globe. The low-cost, lightweight, small and flexible satellites have resulted in a broad range of multi-cube format small satellites, constructed from one to many adjoined cubes, having total mass between 1 and 10 kg. The most challenging design part of the small satellites is to implant a large number of subsystems in a limited space. In order to resolve this issue, the designers are trying to shrink down the subsystem's dimensions further. In this paper, a magnetorquer coil is designed and analyzed for a 4U (4 units cube; 33×33×16.5) cm^3 and 8U (8 units cube; 33×33×33) cm^3 multi-cube small satellites respectively. The coil is embedded in the 6 internal layers of an eight-layers printed circuit board (PCB). The designed magnetorquer system is fully reconfigurable and multiple coils configurations can be achieved by attaching them in series, parallel and hybrid arrangements. Due to embedded nature, the heat generated by the coil may damage the components mounted on the PCB outer surfaces. Therefore, thermal analysis is performed to ensure that the coil generated heat will not cross the PCB components temperature safety limits. All the possible combinations of the coils are analyzed for current drawn, power consumption, heat dissipation, magnetic moment generation and resultant torque. A desired torque can be attained by using a particular coil configuration at the cost of specific amount of consumed power and PCB surface thermals.

Keywords— Satellite, Embedded magnetorquer, magnetic moment, torque, Air-Coil, Multi-Cube

1 INTRODUCTION

Small satellites have recently gained a significant attention in the research community due to their lesser production times and cheaper development costs [1], [2]. These miniaturized satellites are playing substantial role in many fields i.e. navigation, remote sensing, communications and internet etc. Therefore, thousands of these innovative and highly cost-efficient satellites are now being launched from Earth every year. These small satellites are generally categorized by size (e.g. pico-, nano-, micro-satellites etc.) and the number of units that they are comprised of e.g. one-unit (1U), 3-unit (3U), 8-unit (8U) or even multi-cube [3]. Generally, CubeSats are available in a range of various units e.g. 1U, 2U, 3U, or even multi-cube units stacked with each other as shown in Fig. 1. Being cost effective and having lesser development time, many risks are also appended with these tiny bodies i.e. high probability of failure (40%), poor life expectancy and accommodating a large number of critical subsystems of a spacecraft in a small dimension (Swartwout 2016). Along with other numerous risks, attitude control system (ACS) of small spacecraft is also facing challenges i.e. due to smaller and less massive structure make these satellites more vulnerable to environmental disturbance torques such as gravity gradient and aerodynamic torques. So, there is a significant demand for precise attitude control capabilities onboard small satellites. Often, traditional attitude control methods like reaction wheels and thrusters are used but these are excessively expensive in terms of mass, volume, power, and cost for small satellite missions, necessitating alternative approaches. Recently, the use of COTS (commercial off the shelf) based magnetic actuators in low earth orbit (LEO) have been the focus of extensive research [4], [5]. Rapid technological advancements in micro-electromechanical systems (MEMS) have further revolutionized the modularity, diversity and miniaturization of spacecraft. Many universities are working on the next level small satellites that are being launched into space which provide more than just an educational experience [6]–[10]. These students can go out into the community or industry and contribute in a way that was otherwise not possible a decade ago because of the advanced plug & play and adaptable structure.

Since the beginning of space age, magnetic actuation has commonly been used in spacecraft which is dependent on the interaction of the the magnetic field by generated by the satellite's actuators and geo magnetic field. The actuation is provided through the use of active (magnetorquers, reaction wheels or propulsion thrusters) or passive actuators (permanent magnetics, hysteresis rods) [11]. Magnetic actuators are cheap, reliable, have low mass and consume minimum power, while passive actuators are often simple, have no moving parts and require no power but suffers from the disadvantage of inadequate pointing accuracy. The attitude stabilization based on active magnetic actuators represent great challenges, since the magnetic torque for the magnetorquer is constrained on the plane orthogonal to the local direction of geomagnetic field vector while reaction/momentum wheels can generate torque in all the axes but they are bulky and very expensive [12]. Magnetorquers are commonly used to damp the initial angular velocities to a level where the reaction/momentum wheels take over without saturation upon which the magnetorquers are then energized again to de-saturate the motor momentum/reaction wheels [13]. Another major disadvantage of magnetic control is the inherent under-actuation as the torques generated are usually restricted by the processing on-board power available. This under-actuation problem can be addressed by the cross-pollination of magnetic control with gravity gradient stabilization [14]. The use of magnetic control with gravity gradient stabilization is given in [15], [16]. Similarly, in [17]–[19] passive magnets with a set of hysteresis rods are incorporated which lets the vehicle follow local geomagnetic field vector. The challenges these systems face are the control of magnetic forces, unavailability of forces, low attitude accuracies and the implementation of these systems from hardware point of view [20].

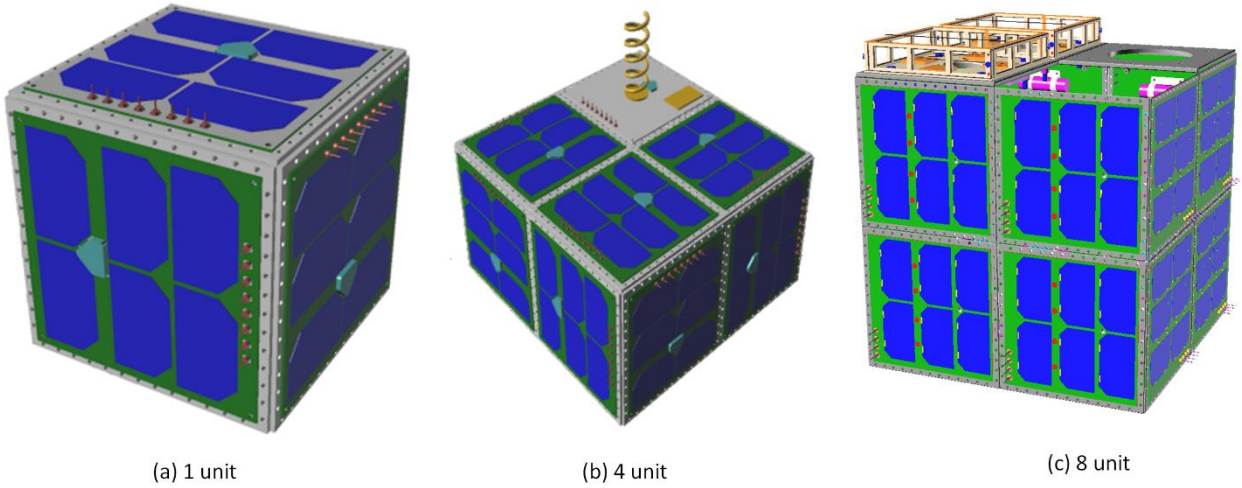

Fig. 1: Single unit and multi-cube small satellites

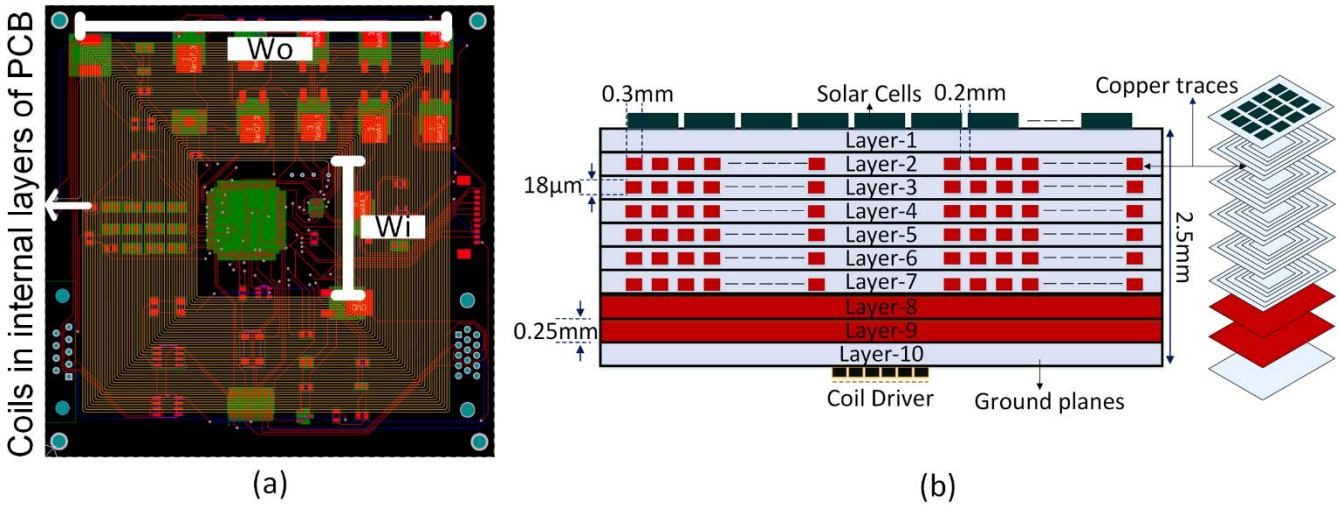

Fig. 2: (a) magnetorquer coil metal traces integrated inside the inner layers of multilayer PCB, (b) cross sectional view of magnetorquer coil in the solar panel PCB

This work proposes miniaturized embedded magnetorquers as shown in Fig. 2 in the form of planar PCB-integrated coils for more demanding multi-cube (4U and 8U cube) small satellites. The actuation capabilities of these integrated magnetorquers for nanosatellites are investigated in [7], [21]–[24] . The problem of multi-cube small satellites rotational
angular velocities having higher inertias is investigated for the proposed embedded magnetorquers. This paper is outlined according to the following pattern. Section 2 introduces the mathematical model of magnetorquer along with its reconfigurable concept and the maneuvering rotation times of different possible coil combinations. In the end, magnetorquers thermal gradients are analyzed to validate the safety of heat transfer and compared with the best-case designs.

2 Magnetorquer Coil System

The magnetorquer coil system level block diagram with respect to on-board computer (OBC) is shown in Fig. 3. Here the block diagram shows all the subsystems related with power management, attitude determination and attitude control. All the electronic components related with various subsystems are embedded on the bottom layer (layer-10) of the PCB whereas the top layer (layer-1) has solar cells. The embedded magnetorquer coil is in the six inner layers (layer-2 ~ layer-7) as shown in Fig. 2. In order to protect the electronic components mounted on layer-10 from the magnetic effects of the coil, two ground plans are added in layer-8 and layer-9, These ground planes work as a shield and protect the layer-10 electronic components from the magnetic effects of the magnetorquer coil. COTS component MSP430 (MSP430F5438A) is used as OBC which is an eight ports (modules) microcontroller. On each module a separate subsystem is attached. Magnetorquer coil is connected on MODULE_E through magnetorquer coil driver. The coil is operated in different modes through the coil driver depending upon the control signals from the OBC. The next subsections describe in detail magnetorquer coil driver and magnetorquer coil.

2.1 Magnetorquer Coil Driver

The coil driver of the magnetorquer unit monitors the amount and direction of current through the coil and ultimately decides the amount of torque generated and direction of satellite spin. It is composed of Allegro A3953 (A3953), differential voltage sensor

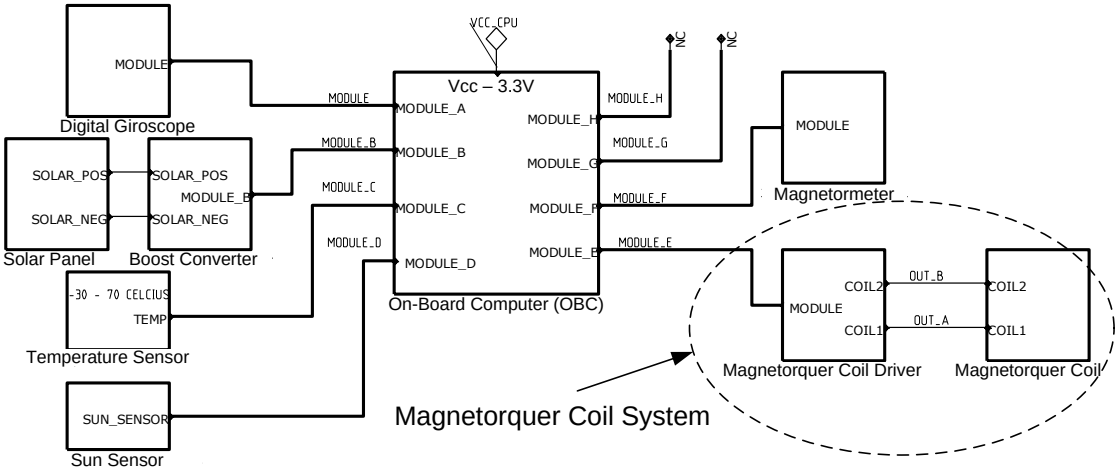

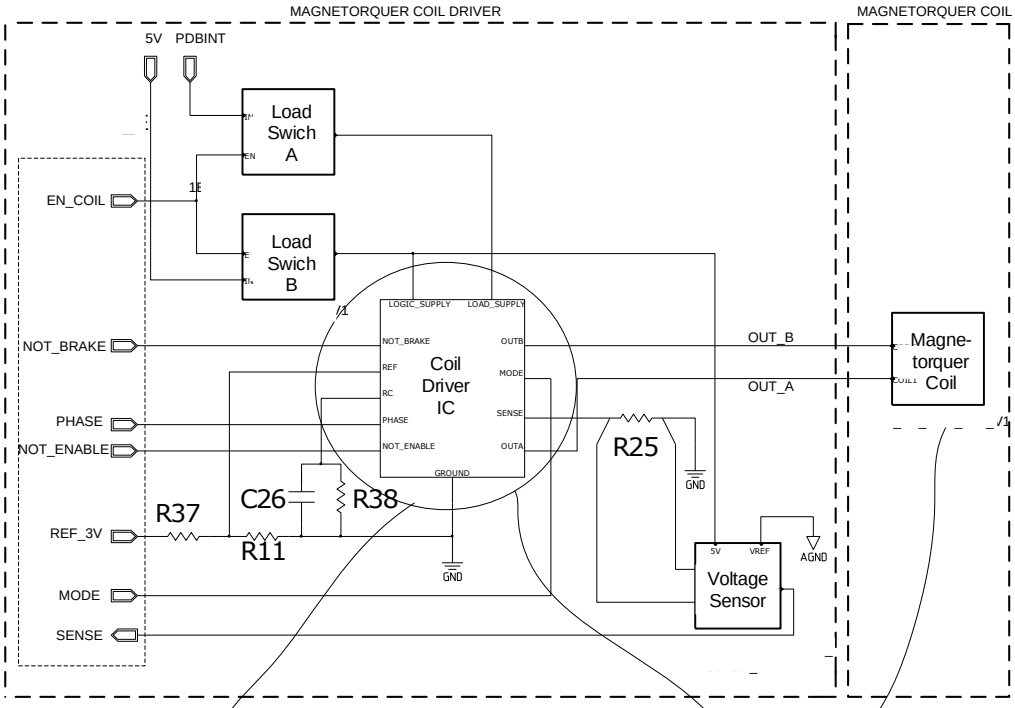

Fig. 4: Schematic of magnetorquer coil system.

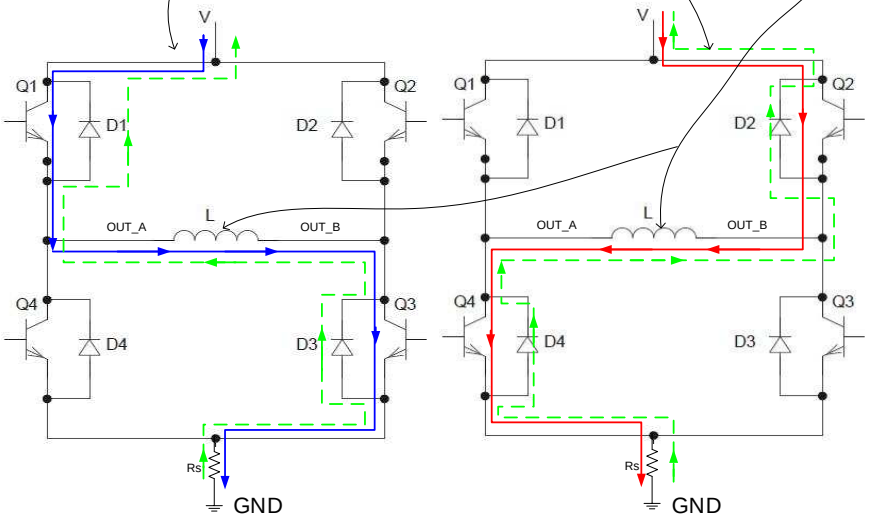

Fig. 5: Coil driver (A3953) internal current paths and coil (L) (a) Forward current flow (b) Reverse current flow.

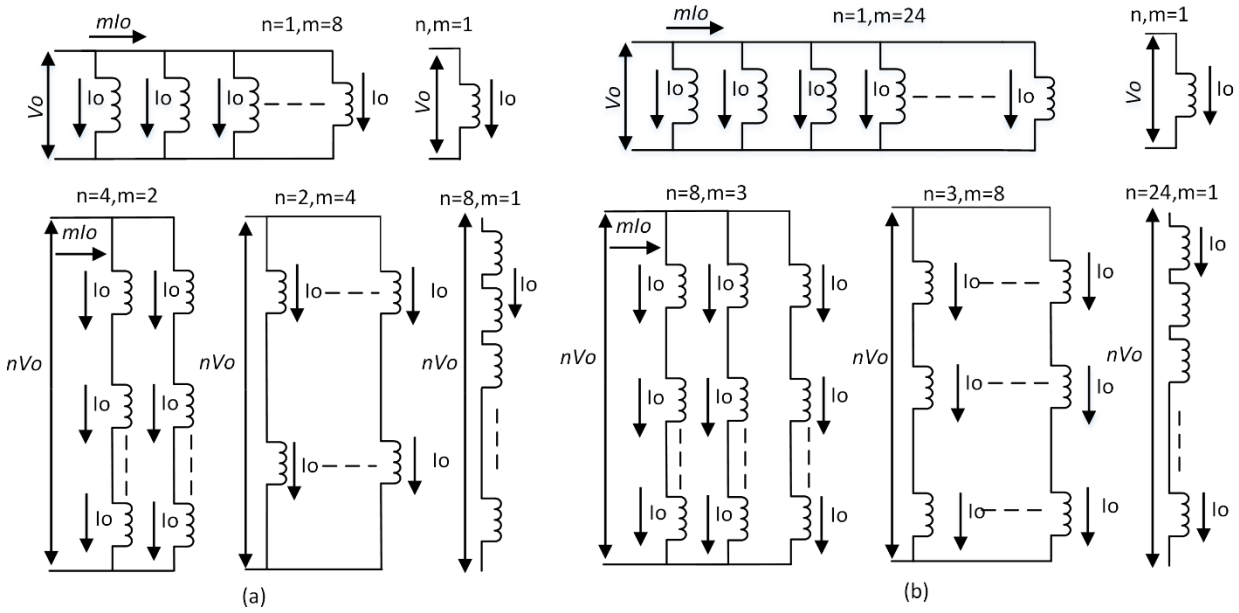

Fig. 6: Voltages required for possible configurations magnetorquer coils providing constant current to 4U (a) and 8U (b) multi-cube satellites

and load switches as shown in Fig. 4. The driver pins OUT_A and OUT_B are connected to two ends of the magnetorquer coil. The pins notBRAKE, PHASE, MODE, NOT_ENABLE and EN_COIL are connected to MODULE_E digital output signals of the tile processor. These signals drive the magnetorquer coil in different modes such as standby, sleep, forward /reverse, brake and fast/slowand current-decay modes. The current flow through the magnetorquer coil is controlled by the differential voltage sensor and sends it to the to the microcontroller which computes the magnetic field and corresponding torque accurately. Load switches terminate the magnetorquer coil power supply on enable signal from OBC.

The topology of the transistor bridge of the magnetorquer coil driver circuitry is illustrated in Fig. 5. The topology of bridge permits bi-directional flow of current through magnetorquer coil (L). Transistors switches Q1 and Q3 permit the flow of current from left to right (illustrated through a solid line from supply 'V' to GND in Fig. 5(a) while transistors switches Q2 and Q4 are switched off at this stage. In reverse current flow case, Q2 and Q4 transistors are switched on and current flows through the coil from right to left (shown through a solid line from supply 'V' to GND in Fig. 5(b). During this stage Q1 and Q3 are switched off. The flyback diodes (D1, D2, D3 and D4) helps in the de-excitation of the copper traces during intermediate resting period as shown through dashed lines in Fig. 5.

3 MAGNETORQUER MATHEMATICAL MODEL

Electromagnetic PCB integrated set of magnetorquer coils operate on the principle of dipole moment induced resulting from the current passing through the windings and its coupling with the geo magnetic field giving a control torque. Magnetic dipole moment is then represented by;

$$\vec{D} = N.S.I.\vec{n} \tag{1}$$

Where *N* denote turns number, *S* represent the area of single turn and *I* gives the current flow in the winding.

The Earth magnetic field fluctuates between 0.15G and 0.45G [25] at an altitude of 800km with inclination angle of 89˚. The time varying Earth magnetic field interacts with the resulting dipole moment of integrated magnetorquers printed in the internal layers of PCB for torque impartment onto the spacecraft for attitude maneuverability which is given by the equation below;

$$\vec{\tau} = D_{coils} \times B^b = -B^b \times D_{coils} \tag{2}$$

Where the magnetic dipole moment column matrix is represented by D_{coils} produced due to every integrated magnetorquer and B^b is the geo magnetic field given in the body frame. Considering the spacecrafts' body fixed frame, the equation for x, y and z components of printed magnetorquer coil is represented as;

$$\begin{bmatrix}\tau_{(x)}\\ \tau_{(y)}\\ \tau_{(z)}\end{bmatrix} = \begin{bmatrix}0 & B_z & B_z\\ -B_z & 0 & B_x\\ B_y & -B_x & 0\end{bmatrix}\begin{bmatrix}D_{(x)}\\ D_{(y)}\\ D_{(z)}\end{bmatrix} \tag{3}$$

For the optimal design selection, a single arbitrary reference axis is taken in our future calculations to simplify the computational complexity. The effective torques generated on the satellite when the magnetic field lines are normal to the reference axis will be considered to simplify the mathematical complexity.

The benefit of the embedded design is the reconfiguration through MOSFET switches based on mission needs according to power ratings, generated magnetic moment, imparted torque, and temperature ratings. The asymmetric coils embedded in the internal layers can be reconfigured in (series, parallel and series-parallel hybrid combination) to maximize or minimize the torque and maximum heat dissipation. The coils can be configured and made compatible with the satellites dimensions by changing the arrangement through the onboard processor at any given time. Single layer design parameters are tabulated in Table.1

Fig. 6(a) depicts the printed asymmetric magnetorquers possible combinations (n-series, m-parallel and n×m hybrid). In case of m parallel connected coils, to flow a constant current (I_0) the applied voltage is the same as (nV_0). Similarly, for series arrangement, the voltage is (nV_0) to draw a current (I_0) through n-series connected magnetorquers. In case of series-parallel hybrid configuration, for the same applied voltage (nV_0), the resulting current is (I_0). Fig. 6(b) illustrates the circuit topology of MOSFET switches which provides reconfiguration to the magnetorquer sub-coils. The magnetic moment $\vec{D}$ of M coils arranged in any possible configuration (n-series, m-parallel, $n \times m$-hybrid) is;

$$\vec{D} = M\overrightarrow{D_0} \tag{4}$$

Correspondingly, consumed power of a single coil is;

$$P_0 = I_0^2 R_0 \quad \because R_0 = \rho \frac{L_t}{A}$$

Dissipated power by *M* coils arranged in any possible configuration (m-parallel, n-series, n × m-hybrid) is;

$$P = MP_0 \tag{5}$$

$$\because I = mI_0\ , V = nV_0\ , M = n \times m$$

The magnetic moment and power dissipation ratio also increase when the number of coils are increased, either in parallel, series or the hybrid combination.

Table 1. Single layer magnetorquer coil design parameters

parameters	values
	4U & 8U
Turns number, N	50
Cross sectional Area of trace, A_T	5.4×10^{-9}m^2
Area occupied by single turn, A_1	0.016m^2
Area occupied by single coil, A	0.8m^2
Average length of single turn, L_1	0.34 m
Average length of Single Coil, L_{avg}	37.4 m
Resistivity of copper trace, ρ	3×10^{-8} Ωm
Single Coil Resistance, R_1	80 ±3 Ω
Distance between two traces, T_W	0.2

4 ROTATIONAL ATTITUDE MANEUVERABILITY

The attitude of a spacecraft is the rearrangement of its spatial orientation relative to a reference system. High spin control rate is needed to maintain the nanosatellite attitude known as spin stabilization. The satellite acts like a gyroscope while it is spun around its axis of symmetry to align with the Earth's inertial reference frame for stabilization [26], [27]. Spinning rate of nanosatellites can be affected due to disturbing torques like gravitational & aerodynamic, eddy currents from the earth's magnetic field and the expansion & contraction of spacecrafts due to extreme temperature difference in orbital changes [28]. These disturbing torques can significantly affect the changes in the moment of inertia and thus the corresponding spin rate. There is also a possibility of an accident occurring due to space debris that could result in uncontrolled tumbling of the satellite at excessive angular rates. The prolonged tumbling at higher angular rates could affect the structural integrity of the nanosatellite and its components as well. Therefore, precise torque is needed for the recovery of satellites intended position in orbit after tumbling.

Imparted torque T and the generated inertia moment J of vehicle is accountable for driving the angular speed ω^o along the major axis of inertia while maneuvering the spacecraft and utilizing the magnetometers to predict the direction and magnitude of geo magnetic field for copper traces excitation. Specific controlled torque produced is required for time interval ($0 \rightarrow T/2$) to increase the satellites angular speed for desired angular distance covered φ. A reaction torque ($-\tau$) of same magnitude proportional to the torqueing time ($T/2 \rightarrow T$) of equal interval is required to stop the spacecraft at desired position.

The rotation times of magnetorquer coils are analyzed for single axis attitude maneuvers using Newton's second law of rotational motion.

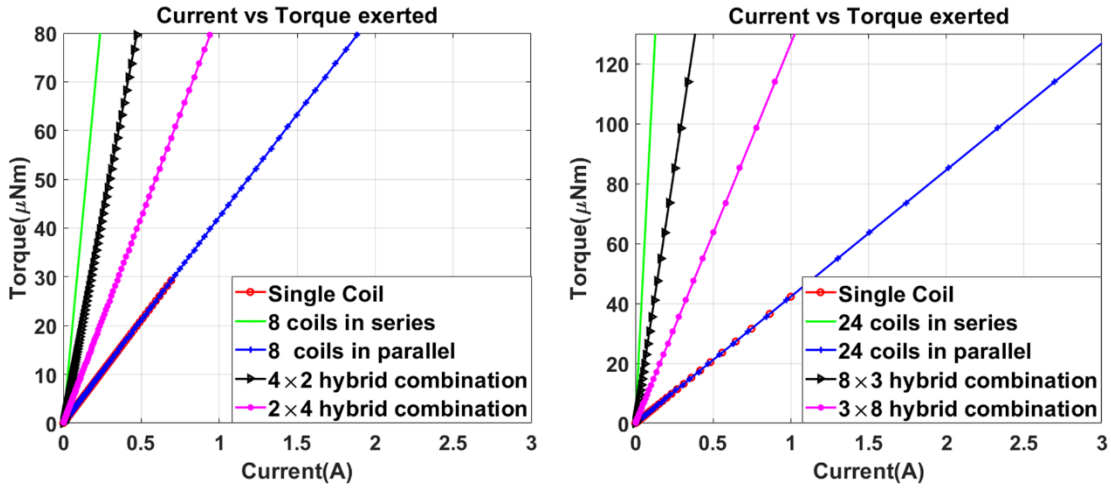

Fig. 7: Current vs generated torque; for the 4U (a) and 8U (b) satellites

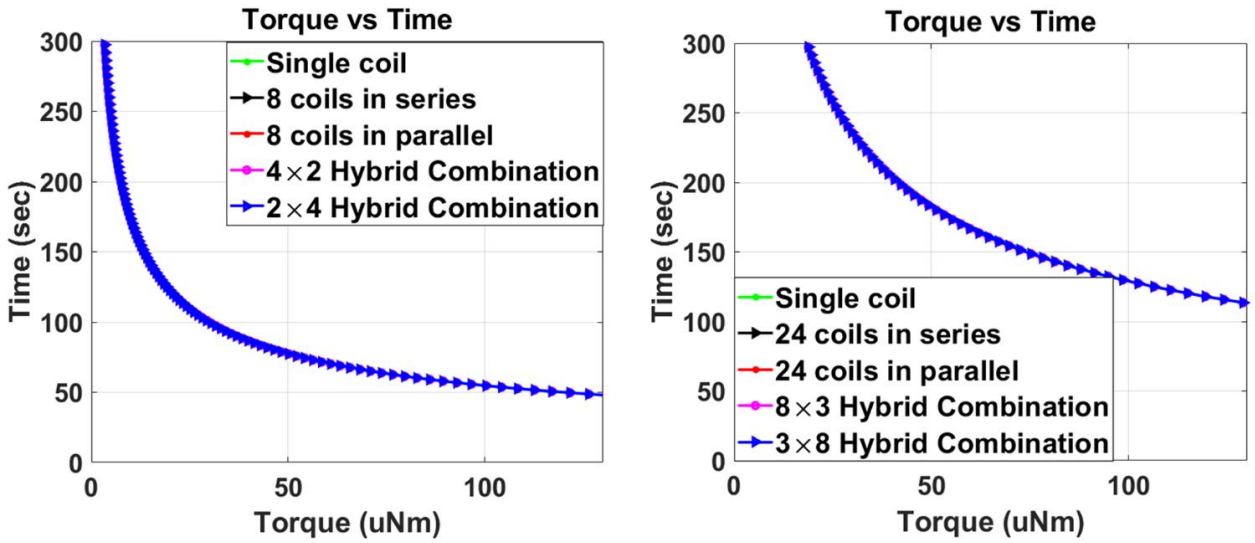

$$\tau = J\omega^{o} \tag{6}$$

Fig. 8: Satellite's rotation time required through an angle of 90˚; for the 4U (a) and 8U (b) satellite

$$\omega^{o} = \int_{0}^{T} \frac{\tau}{J} dt = \int_{0}^{T/2} \frac{\tau_{max}}{J} dt + \int_{T/2}^{T} \frac{-\tau_{max}}{J} dt$$

$$\omega^{o} = \left(\frac{\tau_{max} \cdot t}{J} \Big|_{0}^{T/2} ; \frac{\tau_{max} \cdot (T-t)}{J} \Big|_{T/2}^{T} \right)$$

The angular distance φ is derived from the following equation;

$$\varphi = \int_{0}^{T} \omega^{o} . dt = \left(\frac{\tau_{max} \cdot t^{2}}{2J} \Big|_{0}^{T/2} ; \frac{\tau_{max} \cdot T}{J} \left(t - \frac{t^{2}}{2T} - \frac{T}{4} \right) \Big|_{T/2}^{T} \right) \tag{7}$$

$$\varphi = \omega^{o} \left(\frac{T}{2} \right)^{2} + \omega^{o} \left(\frac{T}{2} \right)^{2} = \frac{\tau}{2J} T^{2}$$

The required time T for the integrated magnetorquer to revolve the satellite for desired angular distance φ can be calculated from (8);

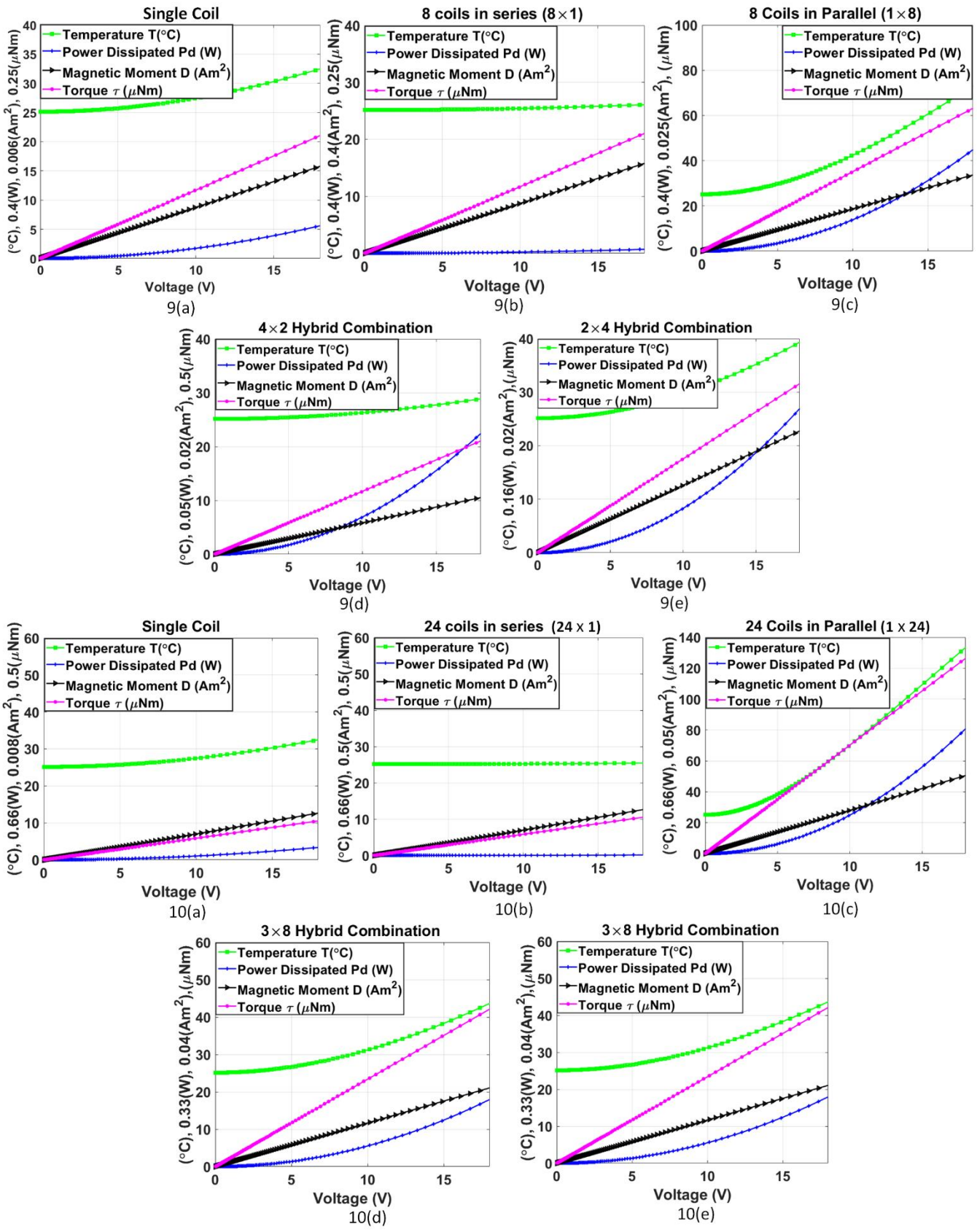

Fig 9-10: (a-e) 4-U and 8-U multi-cube satellites; Plots of magnetic moment, power dissipated and temperature against applied voltage for various coil configurations.

$$T = \sqrt{\frac{2J\varphi}{\tau}} \tag{8}$$

Equation (8) depicts that torqueing time and torque generation needed to revolve the satellite are inversely proportional. The results are plotted for various current inputs as a function of applied voltage to different possible reconfigurable arrangements as shown in Fig. 7. The value of J is set to 0.09 kgm^2 and 0.53 kgm^2 for a 4U and 8U nanosatellite respectively.

For various coil arrangements, the torque imparted on the satellite in presence of 0.5G Earth magnetic field is shown in Fig. 7. The torque generation and the respective time required to rotate the multi-cube nanosatellites by an angle of 90˚ are illustrated in Fig. 8. In case of single or series configuration, generated torque is 5.2 µNm that needs 114.5s and 239s to rotate the spacecraft by an angle of 90˚ for the 4U and 8U multi-cube nanosatellites respectively. In case of parallel configuration, the torque generation is 42.13µNm & 126.3 µNm which needs 84.3s & 114.5s to rotate the spacecraft by an angle of 90˚ for the 4U and 8U multi-cube nanosatellites respectively. The results show that as the cube units of nanosatellites are increased, with the increasing dimensions, the spinning rate proportionally increase. The maximum spinning rate results from the parallel arrangement, but at a cost of high temperature gradient and power consumption. Thermals and power dissipation will be discussed in the next section.

5 THERMAL ANALYSIS

Thermal modeling is the most significant step in the design of printed magnetorquers integrated in the internal layers of the multi layers PCB. When current flow through these coils, power is dissipated which results in PCB surface temperature increase. Thermal analysis is required to ensure that the PCB surface temperature rise should be within the required limits of the components mounted over the PCB. Here we are assuming the system (PCB with embedded magnetorquers) in thermal equilibrium. Which means that the power absorbed by the PCB from the surrounding (P_I) plus the electrical power dissipated by the magnetorquer coils ($P_d = I^2R$) is equal to the total radiated power from the PCB surface to the surrounding (P_o). According to Stefan-Boltzmann's law (Mark Wellons, 2007), the heat radiated from the PCB surface at a specific wavelength is given by $\alpha\sigma {T_o}^4 S$ whereas σ is the Stefan-Boltzmann constant, T_o is the PCB surface temperature, S is the PCB surface area and α is the emissivity. In thermal equilibrium state when zero power is applied to the coils results in $P_o = P_I = \alpha\sigma {T_I}^4 S$where T_I is the surrounding temperature. Comparative thermal analyses for multi-cube small satellites with dimensions 4U (33×33×16.5 cm^3) and 8U (33×33×33 cm^3) have been done by measuring the amount of current (I) that passes through the embedded magnetorquers and the corresponding resistance (R). The integrated coil's power consumption ($P_d = I^2R$) and the corresponding rise of temperature in the PCB is calculated from the derived equations in [7], [21], [22], [29] which are shown below;

$$T_o = \sqrt[4]{\frac{I^2R + \alpha\sigma {T_I}^4 S}{\alpha\sigma S}} \tag{9}$$

Whereas α is the emissivity value photovoltaic panels which is represented in (10)

$$\alpha = \frac{P_d}{\sigma S\left({T_o}^4 - {T_I}^4\right)} \tag{10}$$

Table 2. PCB surface temperature versus applied voltage

Applied Voltage	PCB surface temperature (To (ºC))			
	4U series	4U parallel	8U series	8U parallel
2	27.7	78.8	25.5	103.7
4	39.3	111.4	29.9	146.5
6	48.12	136.4	36.6	179.5
8	55.68	157.5	42.3	207.2
10	62.25	176.1	47.29	231.6
12	68.1	192.8	51.82	253.7
14	73.62	208.3	55.97	274.1
16	78.71	222.5	59.81	293.6
18	83.49	236.1	63.4	310.7

The magnetorquers are excited for a range of 2V~18V inputs such as those used on multi-cube nanosatellites. The plots are depicted in fig 9-10. Here emissivity (α) is assumed to be 0.9 which can be measured through an experimental setup (Ali et al. 2014). The plots show that the printed magnetorquers generate sufficient torque to provide attitude maneuvers for both the cases of 4U and 8U multi-cube small satellites. For 4U spacecraft, the torque generated by the eight coils in series (8×1) is 5.2 µNm with a temperature rise of 25.4˚C while the eight coils in parallel (1×8) generates a torque of 42.1µNm with a temperature increase of 73.18˚C. Similarly, in case of 8U spacecraft, the torque generated by the twenty-four (24×1) coils in series is 5.2 µNm with a temperature rise of 26˚C while the twenty-four (1×24) coils in parallel generates a torque of 126.3µNm with a temperature rise of 133˚C. This shows that, as the dimensions and cube units of spacecraft increase, torque and magnetic moment generation increases while the associated power dissipation and temperature rise subsequently increase, which corresponds to the coil's direct dependence on trace width, size and metal spacing in the module. The analysis shows that the maximum torque to power

dissipation ratio is given by the series configuration which is due to the fact that it draws extremely low current reducing the I^2R losses. The torque to power dissipation ratio also increases with the increase in the cube-unit dimensions of small satellites. The maximum torque results in case of the parallel configuration but at the expense of higher power dissipation and temperature gradient which again corresponds to the higher I^2R losses because of the high current flow.

In order to further clear the picture of PCB surface temperature (*To*) rise in case of various combinations of the coils for 4U and 8U satellite units, *To* values against applied voltage are given in table 2. All these values are measured at room temperature (25ºC). Due to difference in resistance for various coils combinations, the current drawn and resultant power consumed are changing. The larger is the current drawn, the higher is the power consumed and the corresponding increase in *To* values. As the dimension of the satellite increases, the *To* values against the power dissipation also increase. These results reflect that the parallel combinations should be avoided at higher input power because it results in higher PCB temperature.

Based on the magnetic moment generation, torque imparted and power dissipation requirements, the magnetorquer with additional reconfigurability features (24×1, 1×24, 8×3, 3×8, 1×8 and 8×1 etc.) gives more adaptability to the system design by altering the configuration through the onboard processor in real time. The commands from the telemetry processor unit are sent to the onboard computer from ground station for transmission based on the demanded torque and power consumption of the coil. Table 3 tabulates the performance of magnetorquer coils in comparison with the commercial best-case designs.

6 CONCLUSION

This study sought to derive the optimal torque to power dissipation ratios of various possible configurations of pseudo-2D magnetorquer coils for the more demanding multi-cube small satellites. Attitude rotation times and thermal analysis shows that the designed magnetorquers are fully compatible with multi-cube small satellites of higher form factor. Lastly in Table 3, the proposed magnetorquer coils are compared with the commercial best-case designs magnetorquers and prove that they could provide a good alternative to magnetorquer rods and reaction wheels that dominate the CubeSat market today. Future work could involve optimizing the parameters such as the copper thickness, investigating different possible geometric windings and the considerations of temperatures on PCB material of these proposed magnetorquer coils.

Table 3. Comparison of the proposed embedded magnetorquers with the commercial designs

ACS		**Cost**	**Mass (g), +/- 0.25g**	**Dimensions (mm)**	**P (W)**	**τ (µNm)**	**μ (Am^2)**	**$\frac{\tau}{P}$**
Commercial designs	Single-axis reaction wheel (MAI-400)	$7100	110g	33×33 ×38.1	2.2	635	11 mNms	288.8
	Magnetorquer rod (NCTR-M012)	$2000	50 g	94×15×13	0.8	60	1.2	75
Embedded-magnetorquers	(8×1) Series arrangement (4U)	Inside the PCB	Almost massless	Inside the PCB	0.280	5.26	0.1	18.78
	(1×8) Parallel configuration (4U)	Inside the PCB	Almost massless	Inside the PCB	17.9	42.13	0.84	2.3
	(24×1) Series arrangement (8U)	Inside the PCB	Almost massless	Inside the PCB	0.093	5.26	0.09	577.7
	(1×24) Parallel configuration (8U)	Inside the PCB	Almost massless	Inside the PCB	53.9	126.3	2.27	2.3

References

[1] S. Ahmed Khan, A. Ali, Y. Shiyou, and J. Tong, "Reconfigurable Asymmetric Embedded Magnetorquers for Attitude Control of Nanosatellites," *IEEE J. Miniaturization Air Sp. Syst.*, 2021, doi: 10.1109/JMASS.2021.3094232.

[2] S. Ahmed Khan, A. Ali, Y. Shiyou, J. Tong, and J. M. Guerrero, "Optimized Design of Embedded Air Coil for Small Satellites with Various Dimensions," *J. Aerosp. Inf. Syst.*, 2021, doi: 10.2514/1.i010882.

[3] A. Golkar and A. Salado, "Definition of New Space—Expert Survey Results and Key Technology Trends," *IEEE J. Miniaturization Air Sp. Syst.*, 2020, doi: 10.1109/jmass.2020.3045851.

[4] M. O'Halloran, J. G. Hall, and L. Rapanotti, "Safety engineering with COTS components," *Reliab. Eng. Syst. Saf.*, vol. 160, pp. 54–66, 2017, doi: https://doi.org/10.1016/j.ress.2016.11.016.

[5] S. Dahbi *et al.*, "Power budget analysis for a LEO polar orbiting nano-satellite," in *2017 International Conference on Advanced Technologies for Signal and Image Processing (ATSIP)*, 2017, pp. 1–6, doi: 10.1109/ATSIP.2017.8075580.

[6] I. D. Moscholios, V. G. Vassilakis, N. C. Sagias, and M. D. Logothetis, "On Channel Sharing Policies in LEO Mobile Satellite Systems," *IEEE Trans. Aerosp. Electron. Syst.*, 2018, doi: 10.1109/TAES.2018.2798318.

[7] A. Ali, S. A. Khan, M. A. Dildar, H. Ali, and N. Ullah, "Design & thermal modeling of solar panel module with embedded reconfigurable Air-Coil for micro-satellites," *PLoS One*, 2018, doi: 10.1371/journal.pone.0199145.

[8] D. Selva, A. Golkar, O. Korobova, I. L. i Cruz, P. Collopy, and O. L. de Weck, "Distributed Earth Satellite Systems:

What Is Needed to Move Forward?," *J. Aerosp. Inf. Syst.*, vol. 14, no. 8, pp. 412–438, Aug. 2017, doi: 10.2514/1.I010497.
[9] S. Spangelo and J. Cutler, "Analytical Modeling Framework and Applications for Space Communication Networks," *J. Aerosp. Inf. Syst.*, vol. 10, no. 10, pp. 452–466, Oct. 2013, doi: 10.2514/1.I010086.
[10] A. K. Kennedy and K. L. Cahoy, "Performance Analysis of Algorithms for Coordination of Earth Observation by CubeSat Constellations," *J. Aerosp. Inf. Syst.*, vol. 14, no. 8, pp. 451–471, Oct. 2016, doi: 10.2514/1.I010426.
[11] H. S. Ousaloo, "Magnetic attitude control of dynamically unbalanced spinning spacecraft during orbit raising," *J. Aerosp. Eng.*, 2014, doi: 10.1061/(ASCE)AS.1943-5525.0000252.
[12] M. Zhu, X. Chen, and Z. Li, "Attitude and momentum management of inertial oriented spacecraft," *J. Aerosp. Eng.*, 2015, doi: 10.1061/(ASCE)AS.1943-5525.0000471.
[13] F. Giulietti, A. A. Quarta, and P. Tortora, "Optimal control laws for momentum-wheel desaturation using magnetorquers," *J. Guid. Control. Dyn.*, 2006, doi: 10.2514/1.23396.
[14] M. Lovera and A. Astolfi, "Global magnetic attitude control of spacecraft in the presence of gravity gradient," *IEEE Trans. Aerosp. Electron. Syst.*, 2006, doi: 10.1109/TAES.2006.248214.
[15] L. Sun, Z. Wang, G. Zhao, and H. Huang, "Magnetic attitude tracking control of gravity gradient microsatellite in orbital transfer," *Aeronaut. J.*, 2019, doi: 10.1017/aer.2019.112.
[16] K. Zhou, H. Huang, X. Wang, and L. Sun, "Magnetic attitude control for Earth-pointing satellites in the presence of gravity gradient," *Aerosp. Sci. Technol.*, 2017, doi: 10.1016/j.ast.2016.11.003.
[17] M. Y. Ovchinnikov and V. I. Penkov, "Passive magnetic attitude control system for the munin nanosatellite," *Cosm. Res.*, 2002, doi: 10.1023/A:1015197303662.
[18] M. Y. Ovchinnikov, V. D. Shargorodskiy, V. I. Pen'kov, S. A. Mirer, A. D. Guerman, and R. B. Nemuchinskiy, "Nanosatellite REFLECTOR: Choice of parameters of the attitude control system," *Cosm. Res.*, 2007, doi: 10.1134/S0010952507010078.
[19] F. Santoni and M. Zelli, "Passive magnetic attitude stabilization of the UNISAT-4 microsatellite," *Acta Astronaut.*, 2009, doi: 10.1016/j.actaastro.2009.03.012.
[20] K. D. Kumar, M. J. Tahk, and H. C. Bang, "Satellite attitude stabilization using solar radiation pressure and magnetotorquer," *Control Eng. Pract.*, 2009, doi: 10.1016/j.conengprac.2008.07.006.
[21] A. Ali, J. Tong, H. Ali, M. R. Mughal, and L. M. Reyneri, "A Detailed Thermal and Effective Induced Residual Spin Rate Analysis for LEO Small Satellites," *IEEE Access*, 2020, doi: 10.1109/ACCESS.2020.3014643.
[22] A. Ali, K. Ullah, H. U. Rehman, I. Bari, and L. M. Reyneri, "Thermal characterisation analysis and modelling techniques for CubeSat-sized spacecrafts," *Aeronaut. J.*, 2017, doi: 10.1017/aer.2017.108.
[23] A. Ali, M. R. Mughal, H. Ali, and L. Reyneri, "Innovative power management, attitude determination and control tile for CubeSat standard NanoSatellites," *Acta Astronaut.*, 2014, doi: 10.1016/j.actaastro.2013.11.013.
[24] A. Ali, M. R. Mughal, H. Ali, L. M. Reyneri, and M. N. Aman, "Design, implementation, and thermal modeling of embedded reconfigurable magnetorquer system for nanosatellites," *IEEE Trans. Aerosp. Electron. Syst.*, 2015, doi: 10.1109/TAES.2015.130621.
[25] SPENVIS, "Space Enivornment Information System," 2020. https://www.spenvis.oma.be/ (accessed Apr. 03, 2020).
[26] A. Slavinskis *et al.*, "High spin rate magnetic controller for nanosatellites," *Acta Astronaut.*, 2014, doi: 10.1016/j.actaastro.2013.11.014.
[27] H. Ehrpais, J. Kütt, I. Sünter, E. Kulu, A. Slavinskis, and M. Noorma, "Nanosatellite spin-up using magnetic actuators: ESTCube-1 flight results," *Acta Astronaut.*, 2016, doi: 10.1016/j.actaastro.2016.07.032.
[28] V. V Lyubimov and S. V Podkletnova, "Damping of Microsatellite Angular Velocity by Means of Magnetic Moments of Foucault Currents," in *2019 Dynamics of Systems, Mechanisms and Machines (Dynamics)*, 2019, pp. 1–6, doi: 10.1109/Dynamics47113.2019.8944456.
[29] M. R. Mughal, H. Ali, A. Ali, J. Praks, and L. M. Reyneri, "Optimized Design and Thermal Analysis of Printed Magnetorquer for Attitude Control of Reconfigurable Nanosatellites," *IEEE Trans. Aerosp. Electron. Syst.*, 2020, doi: 10.1109/TAES.2019.2933959.
[30] L. Adcole Maryland Aerospace, "MAI-400 single axis reaction wheel assembly," *CubeSatshop*. https://www.cubesatshop.com/wp-content/uploads/2016/06/MAI_Single_Axis_Reaction_Wheel_Assembly-Datasheet.pdf (accessed Jun. 04, 2020).
[31] NCTR-M012, "NCTR-M012 Magnetorquer Rod," *CubeSatShop*. https://www.cubesatshop.com/product/nctr-m012-magnetorquer-rod/ (accessed Jun. 04, 2020).

Embedded Magnetorquer for the more Demanding Multi-Cube Small Satellites

Anwar Ali*, Wang Chao*, Shoaib Ahmed Khan†, Jijun Tong*, Leonardo M. Reyneri
***** School of Information Science and Technology, Zhejiang Sci-Tech University, Hangzhou 310018, China
safi2000pk@gmail.com
† College of Electrical Engineering, Zhejiang University, Hangzhou, 310027, China
Department of Electronics and Telecommunications, Politecnico di Torino, Torino, Italy

***Abstract*—** The recent development in the miniaturization of small satellites and their subsystems has opened a new window of research for the universities around the globe. The low-cost, lightweight, small and flexible satellites have resulted in a broad range of multi-cube format small satellites, constructed from one to many adjoined cubes, having total mass between 1 and 10 kg. The most challenging design part of the small satellites is to implant a large number of subsystems in a limited space. In order to resolve this issue, the designers are trying to shrink down the subsystem's dimensions further. In this paper, a magnetorquer coil is designed and analyzed for a 4U (4 units cube; 33×33×16.5) cm^3 and 8U (8 units cube; 33×33×33) cm^3 multi-cube small satellites respectively. The coil is embedded in the 6 internal layers of an eight-layers printed circuit board (PCB). The designed magnetorquer system is fully reconfigurable and multiple coils configurations can be achieved by attaching them in series, parallel and hybrid arrangements. Due to embedded nature, the heat generated by the coil may damage the components mounted on the PCB outer surfaces. Therefore, thermal analysis is performed to ensure that the coil generated heat will not cross the PCB components temperature safety limits. All the possible combinations of the coils are analyzed for current drawn, power consumption, heat dissipation, magnetic moment generation and resultant torque. A desired torque can be attained by using a particular coil configuration at the cost of specific amount of consumed power and PCB surface thermals.

Keywords— Satellite, Embedded magnetorquer, magnetic moment, torque, Air-Coil, Multi-Cube

1 INTRODUCTION

Small satellites have recently gained a significant attention in the research community due to their lesser production times and cheaper development costs [1], [2]. These miniaturized satellites are playing substantial role in many fields i.e. navigation, remote sensing, communications and internet etc. Therefore, thousands of these innovative and highly cost-efficient satellites are now being launched from Earth every year. These small satellites are generally categorized by size (e.g. pico-, nano-, micro-satellites etc.) and the number of units that they are comprised of e.g. one-unit (1U), 3-unit (3U), 8-unit (8U) or even multi-cube [3]. Generally, CubeSats are available in a range of various units e.g. 1U, 2U, 3U, or even multi-cube units stacked with each other as shown in Fig. 1. Being cost effective and having lesser development time, many risks are also appended with these tiny bodies i.e. high probability of failure (40%), poor life expectancy and accommodating a large number of critical subsystems of a spacecraft in a small dimension (Swartwout 2016). Along with other numerous risks, attitude control system (ACS) of small spacecraft is also facing challenges i.e. due to smaller and less massive structure make these satellites more vulnerable to environmental disturbance torques such as gravity gradient and aerodynamic torques. So, there is a significant demand for precise attitude control capabilities onboard small satellites. Often, traditional attitude control methods like reaction wheels and thrusters are used but these are excessively expensive in terms of mass, volume, power, and cost for small satellite missions, necessitating alternative approaches. Recently, the use of COTS (commercial off the shelf) based magnetic actuators in low earth orbit (LEO) have been the focus of extensive research [4], [5]. Rapid technological advancements in micro-electromechanical systems (MEMS) have further revolutionized the modularity, diversity and miniaturization of spacecraft. Many universities are working on the next level small satellites that are being launched into space which provide more than just an educational experience [6]–[10]. These students can go out into the community or industry and contribute in a way that was otherwise not possible a decade ago because of the advanced plug & play and adaptable structure.

Since the beginning of space age, magnetic actuation has commonly been used in spacecraft which is dependent on the interaction of the the magnetic field by generated by the satellite's actuators and geo magnetic field. The actuation is provided through the use of active (magnetorquers, reaction wheels or propulsion thrusters) or passive actuators (permanent magnetics, hysteresis rods) [11]. Magnetic actuators are cheap, reliable, have low mass and consume minimum power, while passive actuators are often simple, have no moving parts and require no power but suffers from the disadvantage of inadequate pointing accuracy. The attitude stabilization based on active magnetic actuators represent great challenges, since the magnetic torque for the magnetorquer is constrained on the plane orthogonal to the local direction of geomagnetic field vector while reaction/momentum wheels can generate torque in all the axes but they are bulky and very expensive [12]. Magnetorquers are commonly used to damp the initial angular velocities to a level where the reaction/momentum wheels take over without saturation upon which the magnetorquers are then energized again to de-saturate the motor momentum/reaction wheels [13]. Another major disadvantage of magnetic control is the inherent under-actuation as the torques generated are usually restricted by the processing on-board power available. This under-actuation problem can be addressed by the cross-pollination of magnetic control with gravity gradient stabilization [14]. The use of magnetic control with gravity gradient stabilization is given in [15], [16]. Similarly, in [17]–[19] passive magnets with a set of hysteresis rods are incorporated which lets the vehicle follow local geomagnetic field vector. The challenges these systems face are the control of magnetic forces, unavailability of forces, low attitude accuracies and the implementation of these systems from hardware point of view [20].

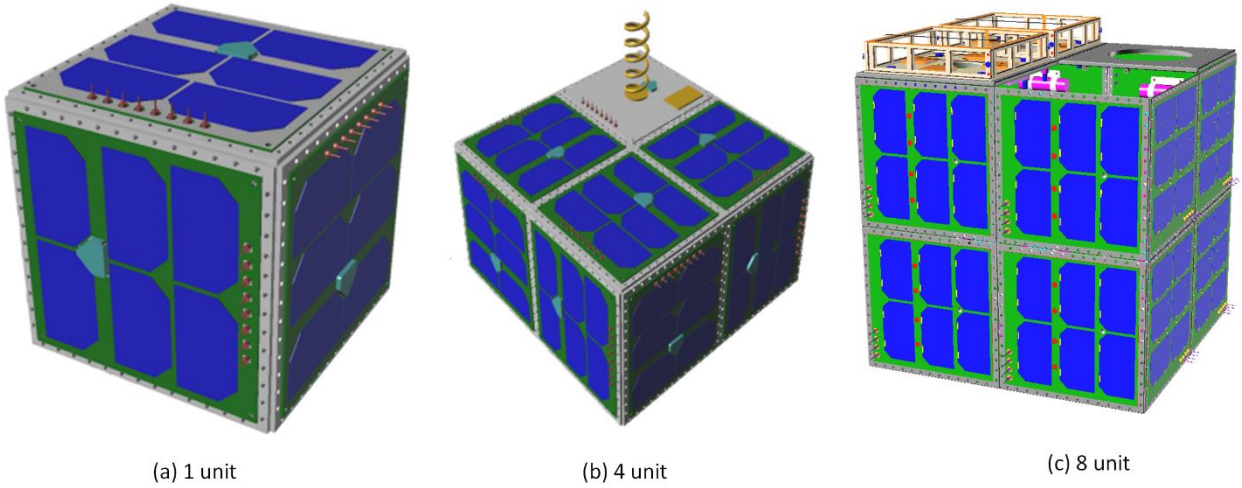

Fig. 1: Single unit and multi-cube small satellites

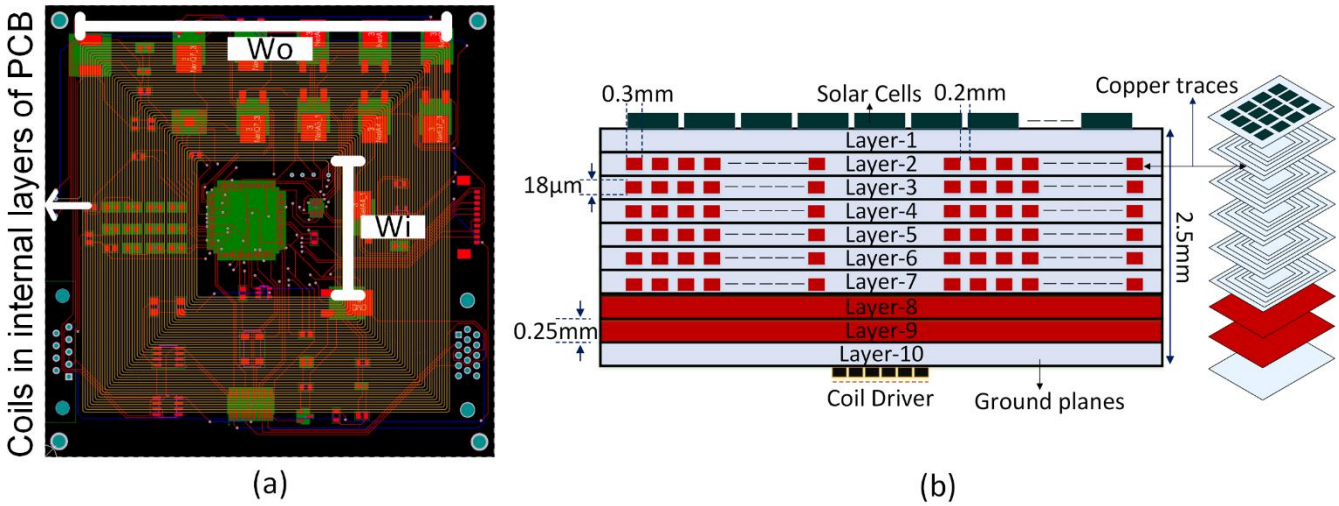

Fig. 2: (a) magnetorquer coil metal traces integrated inside the inner layers of multilayer PCB, (b) cross sectional view of magnetorquer coil in the solar panel PCB

This work proposes miniaturized embedded magnetorquers as shown in Fig. 2 in the form of planar PCB-integrated coils for more demanding multi-cube (4U and 8U cube) small satellites. The actuation capabilities of these integrated magnetorquers for nanosatellites are investigated in [7], [21]–[24] . The problem of multi-cube small satellites rotational
angular velocities having higher inertias is investigated for the proposed embedded magnetorquers. This paper is outlined according to the following pattern. Section 2 introduces the mathematical model of magnetorquer along with its reconfigurable concept and the maneuvering rotation times of different possible coil combinations. In the end, magnetorquers thermal gradients are analyzed to validate the safety of heat transfer and compared with the best-case designs.

2 Magnetorquer Coil System

The magnetorquer coil system level block diagram with respect to on-board computer (OBC) is shown in Fig. 3. Here the block diagram shows all the subsystems related with power management, attitude determination and attitude control. All the electronic components related with various subsystems are embedded on the bottom layer (layer-10) of the PCB whereas the top layer (layer-1) has solar cells. The embedded magnetorquer coil is in the six inner layers (layer-2 ~ layer-7) as shown in Fig. 2. In order to protect the electronic components mounted on layer-10 from the magnetic effects of the coil, two ground plans are added in layer-8 and layer-9, These ground planes work as a shield and protect the layer-10 electronic components from the magnetic effects of the magnetorquer coil. COTS component MSP430 (MSP430F5438A) is used as OBC which is an eight ports (modules) microcontroller. On each module a separate subsystem is attached. Magnetorquer coil is connected on MODULE_E through magnetorquer coil driver. The coil is operated in different modes through the coil driver depending upon the control signals from the OBC. The next subsections describe in detail magnetorquer coil driver and magnetorquer coil.

2.1 Magnetorquer Coil Driver

The coil driver of the magnetorquer unit monitors the amount and direction of current through the coil and ultimately decides the amount of torque generated and direction of satellite spin. It is composed of Allegro A3953 (A3953), differential voltage sensor

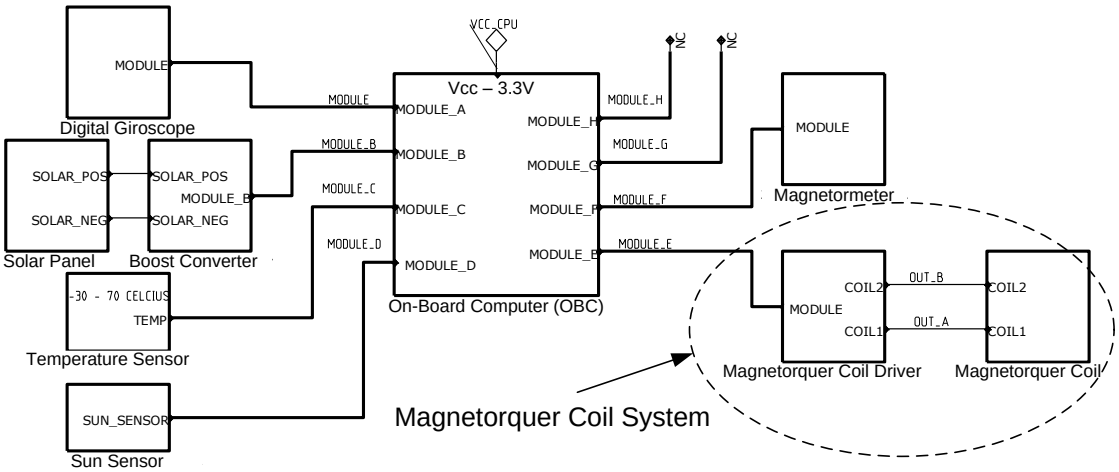

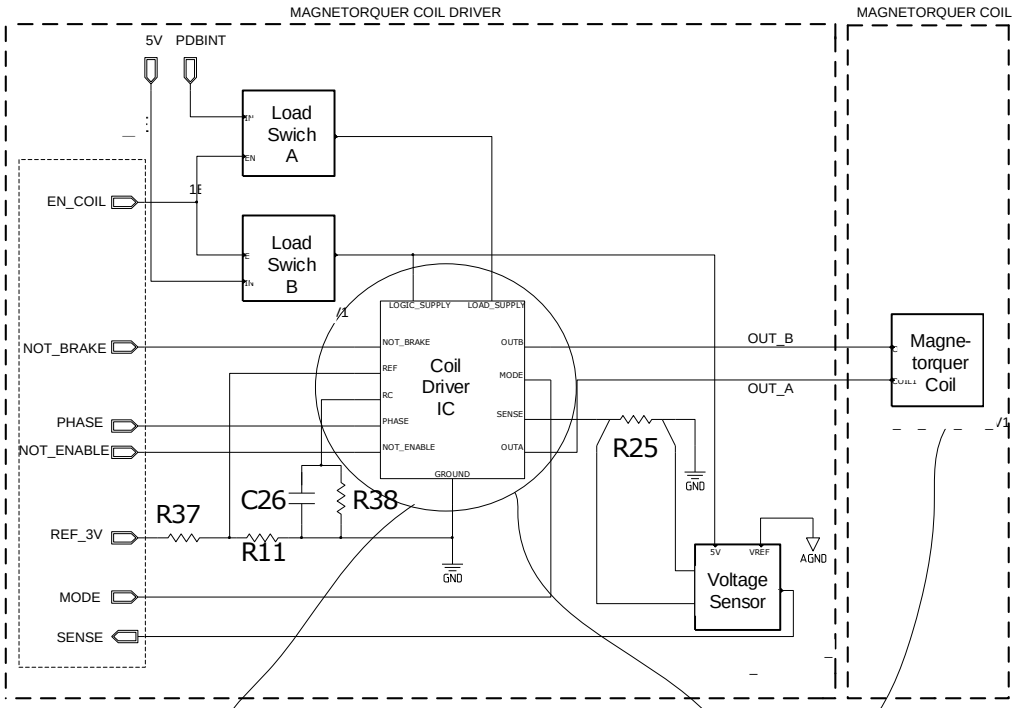

Fig. 4: Schematic of magnetorquer coil system.

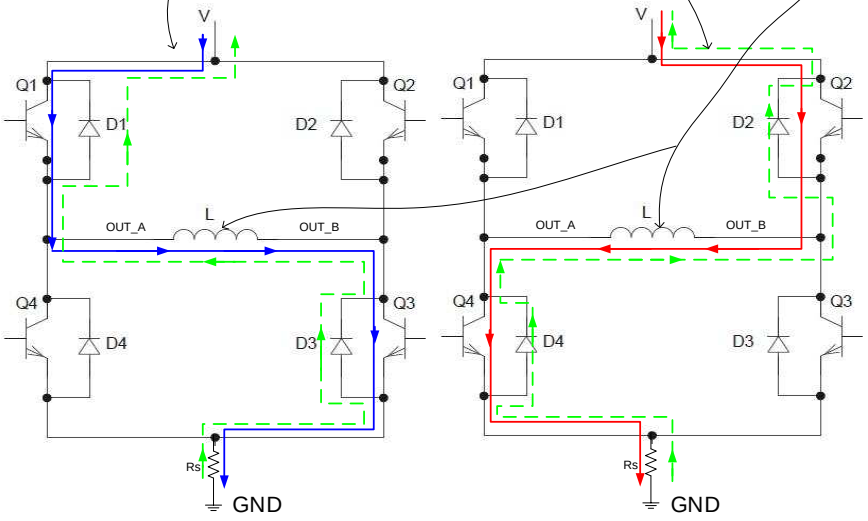

Fig. 5: Coil driver (A3953) internal current paths and coil (L) (a) Forward current flow (b) Reverse current flow.

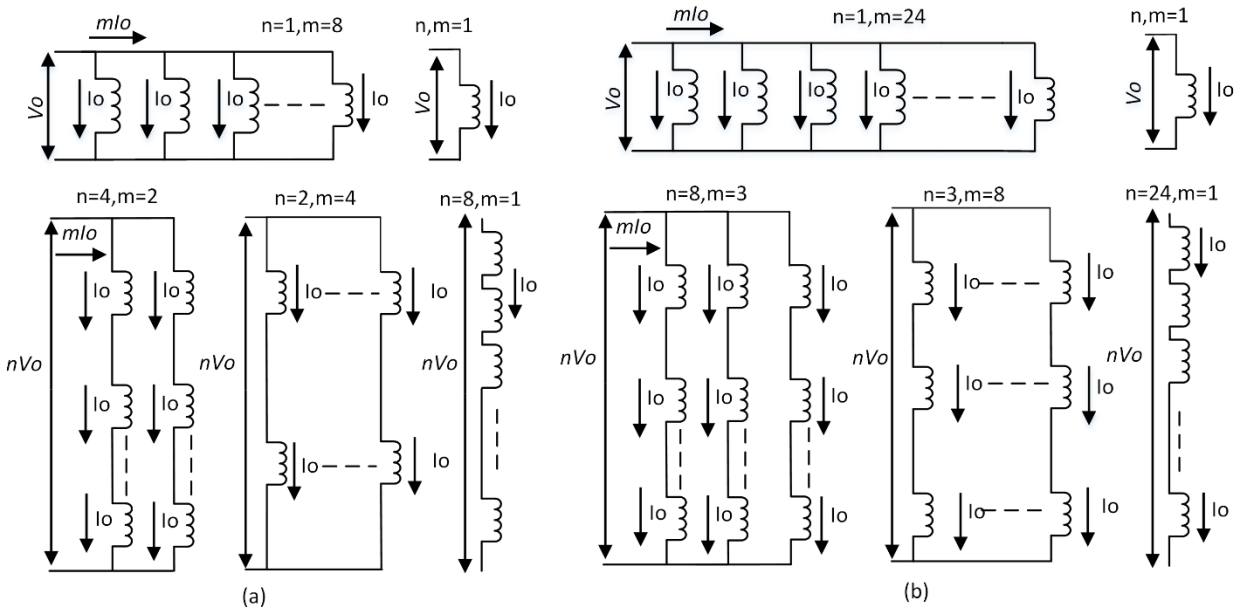

Fig. 6: Voltages required for possible configurations magnetorquer coils providing constant current to 4U (a) and 8U (b) multi-cube satellites

and load switches as shown in Fig. 4. The driver pins OUT_A and OUT_B are connected to two ends of the magnetorquer coil. The pins notBRAKE, PHASE, MODE, NOT_ENABLE and EN_COIL are connected to MODULE_E digital output signals of the tile processor. These signals drive the magnetorquer coil in different modes such as standby, sleep, forward /reverse, brake and fast/slowand current-decay modes. The current flow through the magnetorquer coil is controlled by the differential voltage sensor and sends it to the to the microcontroller which computes the magnetic field and corresponding torque accurately. Load switches terminate the magnetorquer coil power supply on enable signal from OBC.

The topology of the transistor bridge of the magnetorquer coil driver circuitry is illustrated in Fig. 5. The topology of bridge permits bi-directional flow of current through magnetorquer coil (L). Transistors switches Q1 and Q3 permit the flow of current from left to right (illustrated through a solid line from supply 'V' to GND in Fig. 5(a) while transistors switches Q2 and Q4 are switched off at this stage. In reverse current flow case, Q2 and Q4 transistors are switched on and current flows through the coil from right to left (shown through a solid line from supply 'V' to GND in Fig. 5(b). During this stage Q1 and Q3 are switched off. The flyback diodes (D1, D2, D3 and D4) helps in the de-excitation of the copper traces during intermediate resting period as shown through dashed lines in Fig. 5.

3 MAGNETORQUER MATHEMATICAL MODEL

Electromagnetic PCB integrated set of magnetorquer coils operate on the principle of dipole moment induced resulting from the current passing through the windings and its coupling with the geo magnetic field giving a control torque. Magnetic dipole moment is then represented by;

$$\vec{D} = N.S.I.\vec{n} \tag{1}$$

Where *N* denote turns number, *S* represent the area of single turn and *I* gives the current flow in the winding.

The Earth magnetic field fluctuates between 0.15G and 0.45G [25] at an altitude of 800km with inclination angle of 89˚. The time varying Earth magnetic field interacts with the resulting dipole moment of integrated magnetorquers printed in the internal layers of PCB for torque impartment onto the spacecraft for attitude maneuverability which is given by the equation below;

$$\vec{\tau} = D_{coils} \times B^b = -B^b \times D_{coils} \tag{2}$$

Where the magnetic dipole moment column matrix is represented by D_{coils} produced due to every integrated magnetorquer and B^b is the geo magnetic field given in the body frame. Considering the spacecrafts' body fixed frame, the equation for x, y and z components of printed magnetorquer coil is represented as;

$$\begin{bmatrix}\tau_{(x)}\\ \tau_{(y)}\\ \tau_{(z)}\end{bmatrix} = \begin{bmatrix}0 & B_z & B_z\\ -B_z & 0 & B_x\\ B_y & -B_x & 0\end{bmatrix}\begin{bmatrix}D_{(x)}\\ D_{(y)}\\ D_{(z)}\end{bmatrix} \tag{3}$$

For the optimal design selection, a single arbitrary reference axis is taken in our future calculations to simplify the computational complexity. The effective torques generated on the satellite when the magnetic field lines are normal to the reference axis will be considered to simplify the mathematical complexity.

The benefit of the embedded design is the reconfiguration through MOSFET switches based on mission needs according to power ratings, generated magnetic moment, imparted torque, and temperature ratings. The asymmetric coils embedded in the internal layers can be reconfigured in (series, parallel and series-parallel hybrid combination) to maximize or minimize the torque and maximum heat dissipation. The coils can be configured and made compatible with the satellites dimensions by changing the arrangement through the onboard processor at any given time. Single layer design parameters are tabulated in Table.1

Fig. 6(a) depicts the printed asymmetric magnetorquers possible combinations (n-series, m-parallel and n×m hybrid). In case of m parallel connected coils, to flow a constant current (I_0) the applied voltage is the same as (nV_0). Similarly, for series arrangement, the voltage is (nV_0) to draw a current (I_0) through n-series connected magnetorquers. In case of series-parallel hybrid configuration, for the same applied voltage (nV_0), the resulting current is (I_0). Fig. 6(b) illustrates the circuit topology of MOSFET switches which provides reconfiguration to the magnetorquer sub-coils. The magnetic moment $\vec{D}$ of M coils arranged in any possible configuration (n-series, m-parallel, $n \times m$-hybrid) is;

$$\vec{D} = M\overrightarrow{D_0} \tag{4}$$

Correspondingly, consumed power of a single coil is;

$$P_0 = I_0^2 R_0 \quad \because R_0 = \rho \frac{L_t}{A}$$

Dissipated power by *M* coils arranged in any possible configuration (m-parallel, n-series, n × m-hybrid) is;

$$P = MP_0 \tag{5}$$

$$\because I = mI_0\ ,\ V = nV_0\ ,\ M = n \times m$$

The magnetic moment and power dissipation ratio also increase when the number of coils are increased, either in parallel, series or the hybrid combination.

Table 1. Single layer magnetorquer coil design parameters

parameters	values
	4U & 8U
Turns number, N	50
Cross sectional Area of trace, A_T	$5.4 \times 10^{-9}\text{m}^2$
Area occupied by single turn, A_1	0.016m^2
Area occupied by single coil, A	0.8m^2
Average length of single turn, L_1	0.34 m
Average length of Single Coil, L_{avg}	37.4 m
Resistivity of copper trace, ρ	3×10^{-8} Ωm
Single Coil Resistance, R_1	80 ±3 Ω
Distance between two traces, T_W	0.2

4 ROTATIONAL ATTITUDE MANEUVERABILITY

The attitude of a spacecraft is the rearrangement of its spatial orientation relative to a reference system. High spin control rate is needed to maintain the nanosatellite attitude known as spin stabilization. The satellite acts like a gyroscope while it is spun around its axis of symmetry to align with the Earth's inertial reference frame for stabilization [26], [27]. Spinning rate of nanosatellites can be affected due to disturbing torques like gravitational & aerodynamic, eddy currents from the earth's magnetic field and the expansion & contraction of spacecrafts due to extreme temperature difference in orbital changes [28]. These disturbing torques can significantly affect the changes in the moment of inertia and thus the corresponding spin rate. There is also a possibility of an accident occurring due to space debris that could result in uncontrolled tumbling of the satellite at excessive angular rates. The prolonged tumbling at higher angular rates could affect the structural integrity of the nanosatellite and its components as well. Therefore, precise torque is needed for the recovery of satellites intended position in orbit after tumbling.

Imparted torque T and the generated inertia moment J of vehicle is accountable for driving the angular speed ω^o along the major axis of inertia while maneuvering the spacecraft and utilizing the magnetometers to predict the direction and magnitude of geo magnetic field for copper traces excitation. Specific controlled torque produced is required for time interval ($0 \rightarrow T/2$) to increase the satellites angular speed for desired angular distance covered φ. A reaction torque ($-\tau$) of same magnitude proportional to the torqueing time ($T/2 \rightarrow T$) of equal interval is required to stop the spacecraft at desired position.

The rotation times of magnetorquer coils are analyzed for single axis attitude maneuvers using Newton's second law of rotational motion.

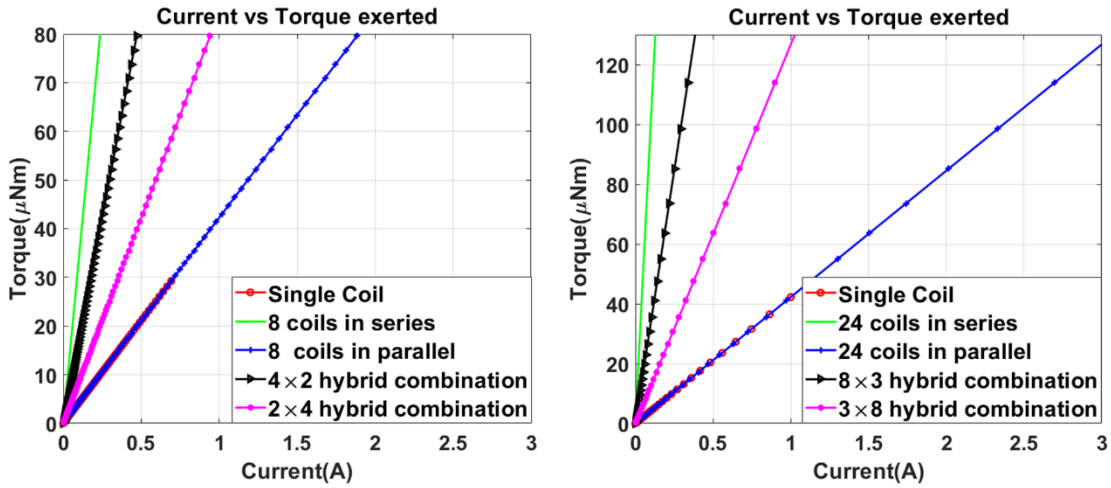

Fig. 7: Current vs generated torque; for the 4U (a) and 8U (b) satellites

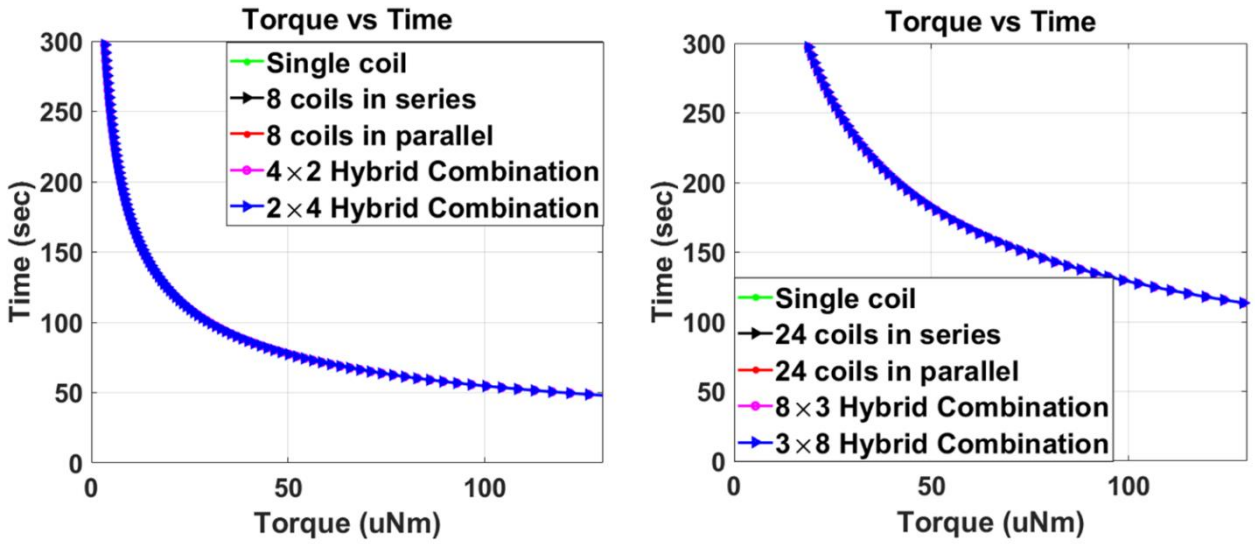

$$\tau = J\omega^{o} \tag{6}$$

Fig. 8: Satellite's rotation time required through an angle of 90˚; for the 4U (a) and 8U (b) satellite

$$\omega^{o} = \int_{0}^{T} \frac{\tau}{J} dt = \int_{0}^{T/2} \frac{\tau_{max}}{J} dt + \int_{T/2}^{T} \frac{-\tau_{max}}{J} dt$$

$$\omega^{o} = \left(\frac{\tau_{max} \cdot t}{J} \Big|_{0}^{T/2} ; \frac{\tau_{max} \cdot (T-t)}{J} \Big|_{T/2}^{T} \right)$$

The angular distance φ is derived from the following equation;

$$\varphi = \int_{0}^{T} \omega^{o} . dt = \left(\frac{\tau_{max} \cdot t^{2}}{2J} \Big|_{0}^{T/2} ; \frac{\tau_{max} \cdot T}{J} \left(t - \frac{t^{2}}{2T} - \frac{T}{4} \right) \Big|_{T/2}^{T} \right) \tag{7}$$

$$\varphi = \omega^{o} \left(\frac{T}{2} \right)^{2} + \omega^{o} \left(\frac{T}{2} \right)^{2} = \frac{\tau}{2J} T^{2}$$

The required time T for the integrated magnetorquer to revolve the satellite for desired angular distance φ can be calculated from (8);

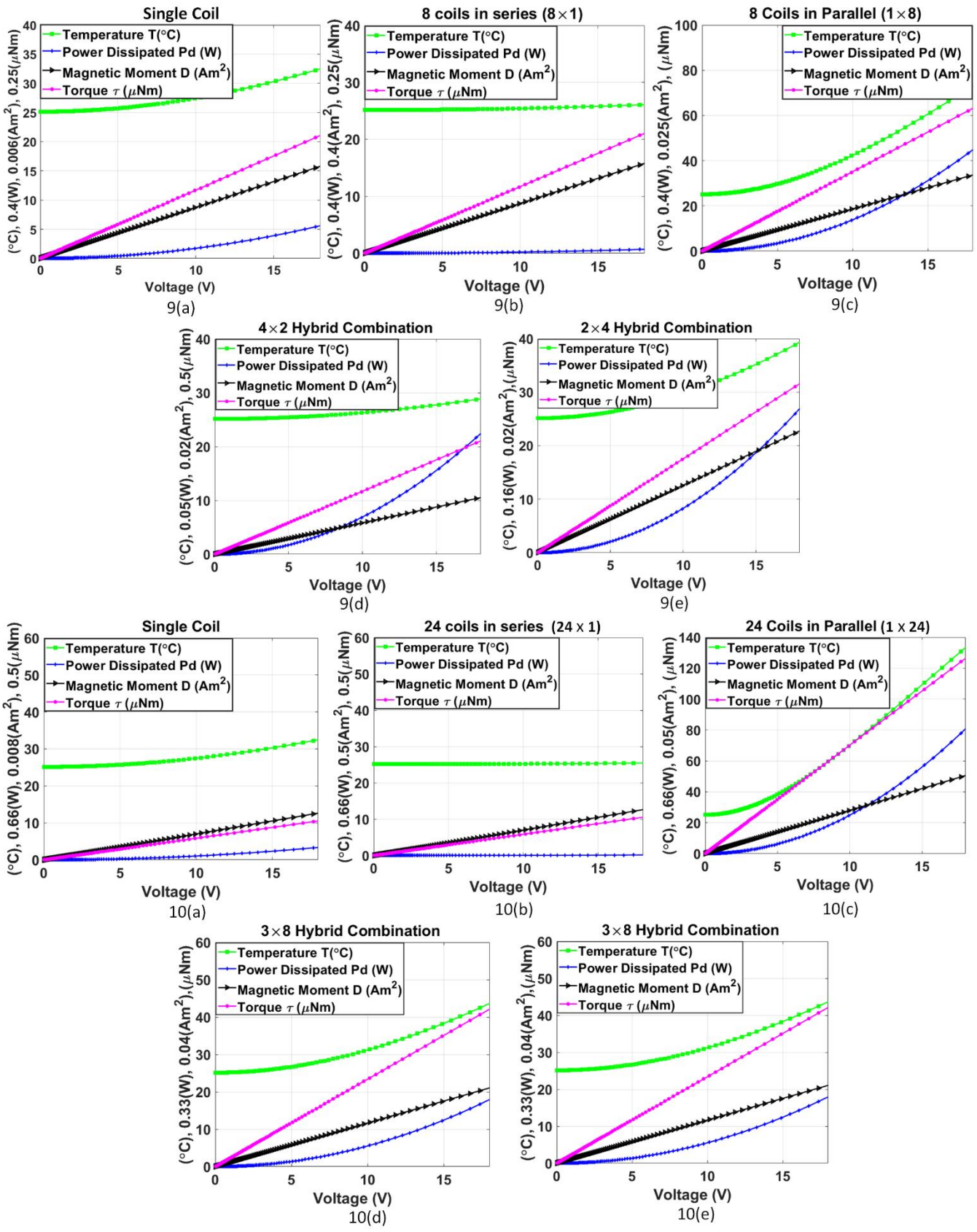

Fig 9-10: (a-e) 4-U and 8-U multi-cube satellites; Plots of magnetic moment, power dissipated and temperature against applied voltage for various coil configurations.

$$T = \sqrt{\frac{2J\varphi}{\tau}} \tag{8}$$

Equation (8) depicts that torqueing time and torque generation needed to revolve the satellite are inversely proportional. The results are plotted for various current inputs as a function of applied voltage to different possible reconfigurable arrangements as shown in Fig. 7. The value of J is set to 0.09 kgm^2 and 0.53 kgm^2 for a 4U and 8U nanosatellite respectively.

For various coil arrangements, the torque imparted on the satellite in presence of 0.5G Earth magnetic field is shown in Fig. 7. The torque generation and the respective time required to rotate the multi-cube nanosatellites by an angle of 90˚ are illustrated in Fig. 8. In case of single or series configuration, generated torque is 5.2 µNm that needs 114.5s and 239s to rotate the spacecraft by an angle of 90˚ for the 4U and 8U multi-cube nanosatellites respectively. In case of parallel configuration, the torque generation is 42.13µNm & 126.3 µNm which needs 84.3s & 114.5s to rotate the spacecraft by an angle of 90˚ for the 4U and 8U multi-cube nanosatellites respectively. The results show that as the cube units of nanosatellites are increased, with the increasing dimensions, the spinning rate proportionally increase. The maximum spinning rate results from the parallel arrangement, but at a cost of high temperature gradient and power consumption. Thermals and power dissipation will be discussed in the next section.

5 THERMAL ANALYSIS

Thermal modeling is the most significant step in the design of printed magnetorquers integrated in the internal layers of the multi layers PCB. When current flow through these coils, power is dissipated which results in PCB surface temperature increase. Thermal analysis is required to ensure that the PCB surface temperature rise should be within the required limits of the components mounted over the PCB. Here we are assuming the system (PCB with embedded magnetorquers) in thermal equilibrium. Which means that the power absorbed by the PCB from the surrounding (P_I) plus the electrical power dissipated by the magnetorquer coils ($P_d = I^2R$) is equal to the total radiated power from the PCB surface to the surrounding (P_o). According to Stefan-Boltzmann's law (Mark Wellons, 2007), the heat radiated from the PCB surface at a specific wavelength is given by $\alpha\sigma {T_o}^4 S$ whereas σ is the Stefan-Boltzmann constant, T_o is the PCB surface temperature, S is the PCB surface area and α is the emissivity. In thermal equilibrium state when zero power is applied to the coils results in $P_o = P_I = \alpha\sigma {T_I}^4 S$where T_I is the surrounding temperature. Comparative thermal analyses for multi-cube small satellites with dimensions 4U (33×33×16.5 cm^3) and 8U (33×33×33 cm^3) have been done by measuring the amount of current (I) that passes through the embedded magnetorquers and the corresponding resistance (R). The integrated coil's power consumption ($P_d = I^2R$) and the corresponding rise of temperature in the PCB is calculated from the derived equations in [7], [21], [22], [29] which are shown below;

$$T_o = \sqrt[4]{\frac{I^2R + \alpha\sigma {T_I}^4 S}{\alpha\sigma S}} \tag{9}$$

Whereas α is the emissivity value photovoltaic panels which is represented in (10)

$$\alpha = \frac{P_d}{\sigma S\left({T_o}^4 - {T_I}^4\right)} \tag{10}$$

Table 2. PCB surface temperature versus applied voltage

Applied Voltage	PCB surface temperature (*To* (ºC))			
	4U series	4U parallel	8U series	8U parallel
2	27.7	78.8	25.5	103.7
4	39.3	111.4	29.9	146.5
6	48.12	136.4	36.6	179.5
8	55.68	157.5	42.3	207.2
10	62.25	176.1	47.29	231.6
12	68.1	192.8	51.82	253.7
14	73.62	208.3	55.97	274.1
16	78.71	222.5	59.81	293.6
18	83.49	236.1	63.4	310.7

The magnetorquers are excited for a range of 2V~18V inputs such as those used on multi-cube nanosatellites. The plots are depicted in fig 9-10. Here emissivity (α) is assumed to be 0.9 which can be measured through an experimental setup (Ali et al. 2014). The plots show that the printed magnetorquers generate sufficient torque to provide attitude maneuvers for both the cases of 4U and 8U multi-cube small satellites. For 4U spacecraft, the torque generated by the eight coils in series (8×1) is 5.2 µNm with a temperature rise of 25.4˚C while the eight coils in parallel (1×8) generates a torque of 42.1µNm with a temperature increase of 73.18˚C. Similarly, in case of 8U spacecraft, the torque generated by the twenty-four (24×1) coils in series is 5.2 µNm with a temperature rise of 26˚C while the twenty-four (1×24) coils in parallel generates a torque of 126.3µNm with a temperature rise of 133˚C. This shows that, as the dimensions and cube units of spacecraft increase, torque and magnetic moment generation increases while the associated power dissipation and temperature rise subsequently increase, which corresponds to the coil's direct dependence on trace width, size and metal spacing in the module. The analysis shows that the maximum torque to power

dissipation ratio is given by the series configuration which is due to the fact that it draws extremely low current reducing the I^2R losses. The torque to power dissipation ratio also increases with the increase in the cube-unit dimensions of small satellites. The maximum torque results in case of the parallel configuration but at the expense of higher power dissipation and temperature gradient which again corresponds to the higher I^2R losses because of the high current flow.

In order to further clear the picture of PCB surface temperature (*To*) rise in case of various combinations of the coils for 4U and 8U satellite units, *To* values against applied voltage are given in table 2. All these values are measured at room temperature (25ºC). Due to difference in resistance for various coils combinations, the current drawn and resultant power consumed are changing. The larger is the current drawn, the higher is the power consumed and the corresponding increase in *To* values. As the dimension of the satellite increases, the *To* values against the power dissipation also increase. These results reflect that the parallel combinations should be avoided at higher input power because it results in higher PCB temperature.

Based on the magnetic moment generation, torque imparted and power dissipation requirements, the magnetorquer with additional reconfigurability features (24×1, 1×24, 8×3, 3×8, 1×8 and 8×1 etc.) gives more adaptability to the system design by altering the configuration through the onboard processor in real time. The commands from the telemetry processor unit are sent to the onboard computer from ground station for transmission based on the demanded torque and power consumption of the coil. Table 3 tabulates the performance of magnetorquer coils in comparison with the commercial best-case designs.

6 CONCLUSION

This study sought to derive the optimal torque to power dissipation ratios of various possible configurations of pseudo-2D magnetorquer coils for the more demanding multi-cube small satellites. Attitude rotation times and thermal analysis shows that the designed magnetorquers are fully compatible with multi-cube small satellites of higher form factor. Lastly in Table 3, the proposed magnetorquer coils are compared with the commercial best-case designs magnetorquers and prove that they could provide a good alternative to magnetorquer rods and reaction wheels that dominate the CubeSat market today. Future work could involve optimizing the parameters such as the copper thickness, investigating different possible geometric windings and the considerations of temperatures on PCB material of these proposed magnetorquer coils.

Table 3. Comparison of the proposed embedded magnetorquers with the commercial designs

ACS		**Cost**	**Mass (g), +/- 0.25g**	**Dimensions (mm)**	**P (W)**	**τ (µNm)**	**μ (Am^2)**	**$\frac{\tau}{P}$**
Commercial designs	Single-axis reaction wheel (MAI-400)	$7100	110g	33×33 ×38.1	2.2	635	11 mNms	288.8
	Magnetorquer rod (NCTR-M012)	$2000	50 g	94×15×13	0.8	60	1.2	75
Embedded-magnetorquers	(8×1) Series arrangement (4U)	Inside the PCB	Almost massless	Inside the PCB	0.280	5.26	0.1	18.78
	(1×8) Parallel configuration (4U)	Inside the PCB	Almost massless	Inside the PCB	17.9	42.13	0.84	2.3
	(24×1) Series arrangement (8U)	Inside the PCB	Almost massless	Inside the PCB	0.093	5.26	0.09	577.7
	(1×24) Parallel configuration (8U)	Inside the PCB	Almost massless	Inside the PCB	53.9	126.3	2.27	2.3

References

[1] S. Ahmed Khan, A. Ali, Y. Shiyou, and J. Tong, "Reconfigurable Asymmetric Embedded Magnetorquers for Attitude Control of Nanosatellites," *IEEE J. Miniaturization Air Sp. Syst.*, 2021, doi: 10.1109/JMASS.2021.3094232.

[2] S. Ahmed Khan, A. Ali, Y. Shiyou, J. Tong, and J. M. Guerrero, "Optimized Design of Embedded Air Coil for Small Satellites with Various Dimensions," *J. Aerosp. Inf. Syst.*, 2021, doi: 10.2514/1.i010882.

[3] A. Golkar and A. Salado, "Definition of New Space—Expert Survey Results and Key Technology Trends," *IEEE J. Miniaturization Air Sp. Syst.*, 2020, doi: 10.1109/jmass.2020.3045851.

[4] M. O'Halloran, J. G. Hall, and L. Rapanotti, "Safety engineering with COTS components," *Reliab. Eng. Syst. Saf.*, vol. 160, pp. 54–66, 2017, doi: https://doi.org/10.1016/j.ress.2016.11.016.

[5] S. Dahbi *et al.*, "Power budget analysis for a LEO polar orbiting nano-satellite," in *2017 International Conference on Advanced Technologies for Signal and Image Processing (ATSIP)*, 2017, pp. 1–6, doi: 10.1109/ATSIP.2017.8075580.

[6] I. D. Moscholios, V. G. Vassilakis, N. C. Sagias, and M. D. Logothetis, "On Channel Sharing Policies in LEO Mobile Satellite Systems," *IEEE Trans. Aerosp. Electron. Syst.*, 2018, doi: 10.1109/TAES.2018.2798318.

[7] A. Ali, S. A. Khan, M. A. Dildar, H. Ali, and N. Ullah, "Design & thermal modeling of solar panel module with embedded reconfigurable Air-Coil for micro-satellites," *PLoS One*, 2018, doi: 10.1371/journal.pone.0199145.

[8] D. Selva, A. Golkar, O. Korobova, I. L. i Cruz, P. Collopy, and O. L. de Weck, "Distributed Earth Satellite Systems:

What Is Needed to Move Forward?," *J. Aerosp. Inf. Syst.*, vol. 14, no. 8, pp. 412–438, Aug. 2017, doi: 10.2514/1.I010497.
[9] S. Spangelo and J. Cutler, "Analytical Modeling Framework and Applications for Space Communication Networks," *J. Aerosp. Inf. Syst.*, vol. 10, no. 10, pp. 452–466, Oct. 2013, doi: 10.2514/1.I010086.
[10] A. K. Kennedy and K. L. Cahoy, "Performance Analysis of Algorithms for Coordination of Earth Observation by CubeSat Constellations," *J. Aerosp. Inf. Syst.*, vol. 14, no. 8, pp. 451–471, Oct. 2016, doi: 10.2514/1.I010426.
[11] H. S. Ousaloo, "Magnetic attitude control of dynamically unbalanced spinning spacecraft during orbit raising," *J. Aerosp. Eng.*, 2014, doi: 10.1061/(ASCE)AS.1943-5525.0000252.
[12] M. Zhu, X. Chen, and Z. Li, "Attitude and momentum management of inertial oriented spacecraft," *J. Aerosp. Eng.*, 2015, doi: 10.1061/(ASCE)AS.1943-5525.0000471.
[13] F. Giulietti, A. A. Quarta, and P. Tortora, "Optimal control laws for momentum-wheel desaturation using magnetorquers," *J. Guid. Control. Dyn.*, 2006, doi: 10.2514/1.23396.
[14] M. Lovera and A. Astolfi, "Global magnetic attitude control of spacecraft in the presence of gravity gradient," *IEEE Trans. Aerosp. Electron. Syst.*, 2006, doi: 10.1109/TAES.2006.248214.
[15] L. Sun, Z. Wang, G. Zhao, and H. Huang, "Magnetic attitude tracking control of gravity gradient microsatellite in orbital transfer," *Aeronaut. J.*, 2019, doi: 10.1017/aer.2019.112.
[16] K. Zhou, H. Huang, X. Wang, and L. Sun, "Magnetic attitude control for Earth-pointing satellites in the presence of gravity gradient," *Aerosp. Sci. Technol.*, 2017, doi: 10.1016/j.ast.2016.11.003.
[17] M. Y. Ovchinnikov and V. I. Penkov, "Passive magnetic attitude control system for the munin nanosatellite," *Cosm. Res.*, 2002, doi: 10.1023/A:1015197303662.
[18] M. Y. Ovchinnikov, V. D. Shargorodskiy, V. I. Pen'kov, S. A. Mirer, A. D. Guerman, and R. B. Nemuchinskiy, "Nanosatellite REFLECTOR: Choice of parameters of the attitude control system," *Cosm. Res.*, 2007, doi: 10.1134/S0010952507010078.
[19] F. Santoni and M. Zelli, "Passive magnetic attitude stabilization of the UNISAT-4 microsatellite," *Acta Astronaut.*, 2009, doi: 10.1016/j.actaastro.2009.03.012.
[20] K. D. Kumar, M. J. Tahk, and H. C. Bang, "Satellite attitude stabilization using solar radiation pressure and magnetotorquer," *Control Eng. Pract.*, 2009, doi: 10.1016/j.conengprac.2008.07.006.
[21] A. Ali, J. Tong, H. Ali, M. R. Mughal, and L. M. Reyneri, "A Detailed Thermal and Effective Induced Residual Spin Rate Analysis for LEO Small Satellites," *IEEE Access*, 2020, doi: 10.1109/ACCESS.2020.3014643.
[22] A. Ali, K. Ullah, H. U. Rehman, I. Bari, and L. M. Reyneri, "Thermal characterisation analysis and modelling techniques for CubeSat-sized spacecrafts," *Aeronaut. J.*, 2017, doi: 10.1017/aer.2017.108.
[23] A. Ali, M. R. Mughal, H. Ali, and L. Reyneri, "Innovative power management, attitude determination and control tile for CubeSat standard NanoSatellites," *Acta Astronaut.*, 2014, doi: 10.1016/j.actaastro.2013.11.013.
[24] A. Ali, M. R. Mughal, H. Ali, L. M. Reyneri, and M. N. Aman, "Design, implementation, and thermal modeling of embedded reconfigurable magnetorquer system for nanosatellites," *IEEE Trans. Aerosp. Electron. Syst.*, 2015, doi: 10.1109/TAES.2015.130621.
[25] SPENVIS, "Space Enivornment Information System," 2020. https://www.spenvis.oma.be/ (accessed Apr. 03, 2020).
[26] A. Slavinskis *et al.*, "High spin rate magnetic controller for nanosatellites," *Acta Astronaut.*, 2014, doi: 10.1016/j.actaastro.2013.11.014.
[27] H. Ehrpais, J. Kütt, I. Sünter, E. Kulu, A. Slavinskis, and M. Noorma, "Nanosatellite spin-up using magnetic actuators: ESTCube-1 flight results," *Acta Astronaut.*, 2016, doi: 10.1016/j.actaastro.2016.07.032.
[28] V. V Lyubimov and S. V Podkletnova, "Damping of Microsatellite Angular Velocity by Means of Magnetic Moments of Foucault Currents," in *2019 Dynamics of Systems, Mechanisms and Machines (Dynamics)*, 2019, pp. 1–6, doi: 10.1109/Dynamics47113.2019.8944456.
[29] M. R. Mughal, H. Ali, A. Ali, J. Praks, and L. M. Reyneri, "Optimized Design and Thermal Analysis of Printed Magnetorquer for Attitude Control of Reconfigurable Nanosatellites," *IEEE Trans. Aerosp. Electron. Syst.*, 2020, doi: 10.1109/TAES.2019.2933959.
[30] L. Adcole Maryland Aerospace, "MAI-400 single axis reaction wheel assembly," *CubeSatshop*. https://www.cubesatshop.com/wp-content/uploads/2016/06/MAI_Single_Axis_Reaction_Wheel_Assembly-Datasheet.pdf (accessed Jun. 04, 2020).
[31] NCTR-M012, "NCTR-M012 Magnetorquer Rod," *CubeSatShop*. https://www.cubesatshop.com/product/nctr-m012-magnetorquer-rod/ (accessed Jun. 04, 2020).